GlobGlacier

Technical Specification (TS)

Prepared by: GlobGlacier consortium





Contract:	21088/07/I-EC
Code:	DUE-GlobGlacier-TS-03
Version:	1.0
Date:	03.03. 2009

Contact:
Frank Paul
Department of Geography
University of Zurich
Winterthurerstr. 190
CH-8057 Zurich

Document status sheet

Version	Date	Changes	Approval
Draft	24.11.2008		
Final	03.03.09	Feedback from the user group & ESA included some updates related to recent developments	

The work described in this report was done under ESA contract 21088/07/I-EC. Responsibility for the contents resides in the authors that prepared it.

Author team:
GIUZ: Frank Paul; Holger Frey; GUIO: Andreas Kääb, Kimberly Casey; Enveo: Thomas Nagler, Helmut Rott, Gabriele Bippus; SGUE: Andrew Shepherd, Eero Rinne; Gamma: Tazio Strozzi

GlobGlacier Technical Officer at ESA:
Frank Martin Seifert

Table of Contents

1. Purpose

This document is the Technical Specification (TS) of the GlobGlacier project. According to the Statement of Work (SoW) and the project proposal, the purpose of the TS is to provide a technical answer to the Requirements Baseline (RB). The TS is a detailed description of the generated products and their processing in support of the user group. Among others, the TS provides:

(a) a detailed description of the required components (input, processing, output);
(b) detailed processing workflows and algorithm descriptions for each sensor under consideration and generated product;
(c) possibilities and requirements for product validation;
(d) a description of the integrated information products and its formats;
(e) consolidation of the demonstration cases to be carried out in phase 2.

Product generation will be compliant with the standards and product specifications (e.g. by GLIMS, WGMS, UNESCO) as given in the appendix of the RB. These documents also describe the required metadata files and ancillary information. Because products will be provided to the respective data hosts (GLIMS/WGMS database) on a case-by-case basis, a generally applicable data transfer interface is not developed. This document complements the GLIMS analysis tutorial by Raup and Khalsa (2007) as it specifically describes the methods applied whithin the GlobGlacier project. During the second progress meeting in Innsbruck product integration and data formats were discussed. A summary of these specifications is included in the TS. Accuracy measures will be discussed in the forthcoming document deliverable 6 (Acceptance Test Document). prescriptive

This document starts with a detailed description of points (a), (b) and (c) for each product and the used sensors. It is followed by points (d) and (e) and closes with some examples in the Appendix to better illustrate what the output of the respective methods is.

2. Workflows and algorithms

2.1 Glacier outlines

The data processing scheme for the glacier outlines product has been divided into a pre-, main- and post-processing stage. While the pre-processing mainly depends on the data source and the used software, the main processing varies with the sensor and the post-processing with the level of the generated product. The steps are schematically summarized in Fig. 1 and discussed in detail below. A processing example in Chapter 4 illustrates the used algorithms.

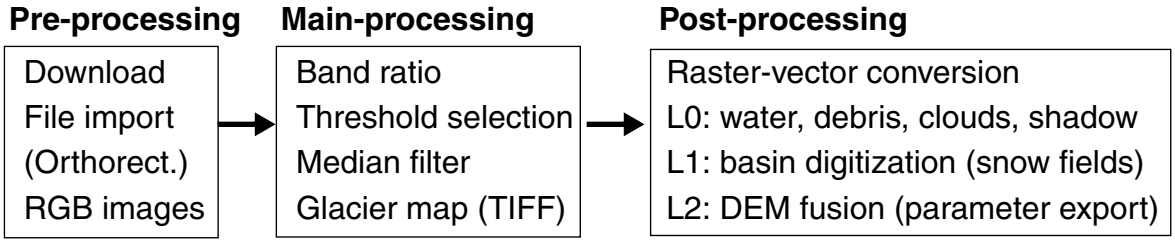

Fig. 1: Schematic overview of the data processing steps for the glacier outline products.

2.1.1 Pre-processing

The pre-processing is described here for the software package PCI geomatica (v9.1) and the data formats GeoTiff (Landsat/SPOT) and HDF (ASTER). Further software products / data formats are described in document deliverable 5 (DDF). An overview of the principal pre-processing steps is given in Fig. 2.

The major data source for the glacier outlines product is the Landsat satellite where already orthorectified data could be obtained for free from USGS/NASA ftp-sites (ASTER/SPOT data are mainly used for DEM generation, see 2.4). The available datasets include quicklooks in two band combinations and two resolutions, metadata files, and a compressed GeoTiff for each image band (MSS: 4 files, TM: 7 files, ETM: 9 files). A selection of scenes could be downloaded from the GLCF server while the USGS data holdings are available for free download from the glovis.usgs.gov data browser. For generating glacier outlines only the first five TM/ETM+ bands (all MSS bands) are required. It is assumed in the following that already orthorectified and optimal scenes for glacier mapping have been selected, i.e. from the end of the ablation period with as little seasonal snow as possible and cloud free conditions.

After downloading of the files for an individual scene, the image bands have to be uncompressed. This gives a set of tif files which have stored the information on the geolocation, projection, datum and pixel size internally in an image header. When these files are converted to the format of the used image processing system (.pix in the case of PCI), these information is

read and applied to each band. For PCI, each band is imported into a separate .pix file (b1.pix, b2.pix, ..., b5.pix). The raw GeoTiff files from each image band could also be converted to a raster format for further processing in a GIS.

In PCI the b1.pix is extended by six more 8-bit channels (which can store values between 0 and 255) using the command `PCIMOD` in the `EASI` environment (as a question about disk space have to be quoted by typing 'Y'). Finally, the bands 2-5 are transferred to the channels 2-5 of the file b1.pix. In order to save disk space, all tif and the b2.pix-b5.pix files can be deleted and the b1.pix file should get a proper name including path/row and acquisition date.

A further step during pre-processing is the generation of colour composites using the band combinations (for Landsat TM/ETM+): 3, 2, 1 (as RGB) for corrections of shadow zones and lakes, 432 for trimline and ice divide mapping, and 543 for detection of clouds and visual control of the glacier outlines (including debris cover). Export in the GeoTif format allow digital overlay in a GIS. Several public domain and commercial image processing systems are available to perform contrast enhancements of the respective composites. The 321 composite should be optimized to clearly discern ice and snow in cast shadow (which will generally lead to saturated snow/ice surfaces in sunlight), while the 432 composite should reveal subtle illumination differences in such sunlit ice/snow zones (and will thus be very dark in regions of cast shadow). The contrast stretch of the 543 composite is less critical, but ice and snow in shadow should still be visible.

1. Quicklook browser

- visual analysis of scenes (clouds, snow conditions)
- download of quicklooks, comparison and selection
- download of images and metadata files

2. Image processing software

- convert bands to single image in software specific format
- create RGB images (321, 432, 543) for overlay/correction

Fig. 2: Principal steps for pre-processing for each scene in each key region.

2.1.2 Main processing

General remarks

The main processing depends on the available image bands and thus on the sensor under consideration. The required image processing commands like noise reduction with a 3 by 3 (kernel size) median filter and basic image math (+, -, /) are available from all software products and are thus not detailed here with their specific commands. Most useful is to write the glacier mapping workflow in small scripts (see Chapter 4), where only individual parameters (i.e.

2.1 Glacier outlines

thresholds) have to be changed to optimize the classification. In order to store the used threshold values, each scene has its own script. As described in the Requirements Baseline (RB), the method used for to classification of glaciers in GlobGlacier is based on thresholded ratio images. Other methods are of similar quality (e.g. the normalized difference snow index, NDSI) but are not described here as they require further calculations and are thus somewhat less efficient (cf. Paul et al., 2002; Paul and Kääb, 2005). The automated mapping requires at least one band in the shortwave infrared (SWIR) where the reflectance of ice and snow is very low compared to the red or near infrared bands. The band ratio works on raw digital numbers which means that no further correction (e.g. of atmospheric or topographic effects) is required. In Fig. 3 the processing is summarized schematically. When a fully manual digitization is applied, the GLIMS analysis tutorial by Raup and Khalsa (2007) should be used as a guide.

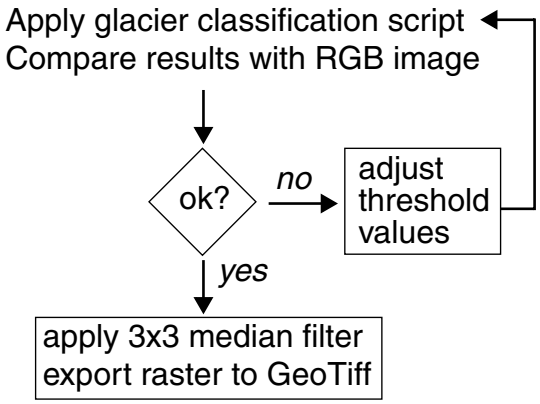

Fig. 3: Schematic workflow of the main image processing steps for glacier mapping.

In principal, the ratios NIR/SWIR or red/SWIR perform equally well but have characteristic advantages and disadvantages. Both ratios wrongly classify turbid lakes as glacier ice, but much more pronounced for the red/SWIR ratio. While the red/SWIR ratio wrongly maps regions in shadow without snow and ice, the NIR/SWIR ratio misclassifies vegetation in shadow (e.g. Paul et al., 2002). While the correction of the former is possible with an additional threshold in the blue or green band, the latter could be corrected by a calculating a map of vegetation covered regions (e.g. using the Normalized Difference Vegetation Index, NDVI) and subtracting it from the glacier map. The disadvantage of the NIR/SWIR ratio could be an exclusion of all regions in shadow, even when ice or snow is present. This could occur for low solar elevations (deep shadows) or a very clean atmosphere. From this point of view, it was decided to use in GlobGlacier the red/SWIR ratio with an additional threshold in the blue (TM/ETM+) or green (ASTER/SPOT) band throughout.

Ratio images

The threshold value for the ratio is very robust (mostly between 1.6 and 2.4) and a good starting value that works well in most cases is 2.0. The shadow mapping is much more sensitive to the threshold value and depends strongly on atmospheric conditions, solar elevation, fresh

snow cover on adjacent slopes etc., and have to be found iteratively by visual comparison. Typical values range from 30 to 70 DNs and a good starting value is 50. The first principle for the selection of the respective threshold value is to minimise the workload for post-processing (i.e manual editing). As debris cover, lakes (turbid or frozen) have to be corrected manually anyway, it is most useful to optimize the mapping in regions of cast shadow. They are also most sensitive for both thresholds so the test regions for visual comparisons and threshold optimization should be selected at such sites in shadow. When passing a certain threshold (which generally is sharply defined) in the blue (green) band it is not possible to map more snow/ice in shadow without increasing the number of mapped pixels in shadow regions without snow/ice at the same time. In such a case the optimal threshold has been found. It is recommended to map snow/ice in black on a white background for improved visual perception.

Median Filter
Spatial filters could be used to reduce high spatial variability or noise. In particular ratio images are sensitive to such noise as small differences in DNs are strongly enhanced. In the case of Landsat images from GLCF that are interpolated by nearest neighbour (NN) resampling during orthorectification, a median filter (3 by 3 kernel size) is applied to band 5 before the ratioing is performed. This is not necessary when cubic convolution (CC) resampled images are used. The same filter could also be applied to the classified glacier map. While the filter clearly helps to reduce misclassification due to noise (in shadow regions), debris cover (isolated pixel gaps) and small snow patches, mountain ridges and rock outcrops are closed at the same time and very small glaciers (<0.1 km^2) are decreased in size (Paul et al., 2003). This has to be considered for the selection of the threshold value as well as for the required post-processing (i.e. editing small glaciers). Considering the scenes that have been processed so far, the application of a median filter could clearly be recommended (see example in Chapter 4).

MSS
Approaches to classify glaciers from MSS bands (i.e. without the SWIR) band do also exist, but are not described here in detail (see Svoboda and Paul, in press). Within the framework of GlobGlacier, MSS satellite scenes are mainly used to determine changes in terminus position (length changes) rather than mapping the entire glacier. Contrast enhanced false colour composites allow in most cases a good identification of the terminus. Due to the coarser pixel size of the MSS sensor (80 by 80 m), the accuracy of the derived length changes is reduced (Hall et al., 2003) and thus preferably applied to glaciers of sufficient size.

Landsat (TM/ETM+)
The method for glacier mapping with the spectral bands from the TM/ETM+ sensors is illustrated in Chapter 4. The result of the band ratio after threshold application (snow/ice=0, other=255) is written to channel 7 of the pix file (channel 6 might store the median filtered band 5) and compared to close-ups of various band combinations for optimization of the result. The final classification is then median filtered with the result going into channel 6 (overwriting the former median filtered band 5) and exported to a GeoTiff file for further processing. An RGB composite with the filtered and unfiltered results will reveal the influence of the filter and allows to evaluate its use.

ASTER
In principal, the same method as described for Landsat could be applied to map glaciers with ASTER data, but three points have to be considered. (1) ASTER has no blue band so that the additional threshold for the shadow mapping has to rely on the green band. (2) The spatial resolution from the SWIR band (30 m) is different from the VNIR bands (15 m) and has to be resampled (bilinear) to 15 m resolution at first. (3) The gain settings of the ASTER sensor could vary from scene to scene to improve the radiometric performance over highly reflective surfaces like snow. Such a lowered gain over glacierized regions decrease the reflectance in cast shadow considerably and could result in the impossibility to map snow/ice here. But as the major use of ASTER data in GlobGlacier is DEM generation, the lowered gain settings help to improve the accuracy of the DEM over snow surfaces considerably. Gaps in regions of cast shadow have to be taken into account nevertheless. An examples of image processing with ASTER is also given in Chapter 4.

SPOT
The spectral bands of SPOT are similar to ASTER (no blue band), but all relevant multispectral bands have 20 m spatial resolution throughout. The higher resolution of the pan-chromatic bands (10 m for SPOT4, up to 2.5 m for SPOT5) helps to track subtle features more accurately. For this reason the pan-band is mainly used for manual delineation and validation of glacier outlines as derived by the Landsat sensors.

2.1.3 Post-processing

Major steps of the post-processing are illustrated schematically in Fig. 4. At first, the classified image (GeoTiff) has to be converted to vector outlines. This part of the processing could be done within a GIS. The principle steps are: (1) transform the GeoTiff image to a raster format, (2) assign a no-data flag to non-glacier areas and (3) convert the grid to vector outlines with polygon topology. Similar processing steps could be performed in most GIS software products. The obtained glacier outlines should be copied to a working file in which the corrections are applied. In the case of huge lakes, rivers or ocean water (probably with sea ice or icebergs) in the image, gross classification errors should be corrected first to reduce the number of polygons (could be more than 50 000). This could be quickly done by selecting the respective regions within a roughly digitized polygon and delete them.

L0 outlines (L0)
The L0 glacier outlines should depict all glaciers (incl. perennial snow banks) in a scene without discriminating individual entities where glaciers are in contact (e.g. emerging from an ice-cap or icefield). This requires to correct misclassification in regions with lakes/water, clouds and debris cover. The correction of lakes is straight forward as they are clearly visible in the 321 composite image. The calving terminus is digitized from shore to shore and only includes the connected parts. Disconnected iceflows are not digitized although they might still have a connection to the main glacier under the water. In the case of frozen lakes or fjords the identification of the calving front could be more difficult but is in most cases still possible. While several automated methods for detection of lakes (with differing turbidity) are available, they

2.1 Glacier outlines

often have problems in mapping all degrees of turbidity at the same time without wrongly classifying glaciers as lakes. Lakes in shadow are also not included (cf. Huggel et al., 2002). Moreover, lakes could be located on the glacier surface (e.g. melt ponds) and should then be part of the glacier. For this reason it was decided to detach and remove lakes/water by manual editing.

Debris-covered glaciers are widespread in high-mountain topography with strong weathering and (optically thick) debris could cover more than 50% of a glacier. These regions must thus be appended to the automatically classified part. In this context we refer to debris that covers the underlaying ice completely, independent of its thickness. If some bare ice is still visible from above (averaged over the pixel size of the sensor) the glacier mapping with the band ratio is often able to classify this correctly. Vertically thick but horizontally thin medial moraines are closed by the median filter. Automated methods for mapping debris covered parts have been developed (e.g. Bishop et al., 2001; Paul et al., 2004), but a DEM and visual inspection/correction of the results is required nevertheless. Actually, automated mapping of debris-covered glaciers is still a hot topic in research and forms the major bottleneck for rapid automated glacier mapping (e.g. Racoviteanu et al., in press). For this reason, debris covered parts are delineated manually in GlobGlacier using contrast enhanced imagery in the background. In some regions the results from automated techniques will be used as a guide for the manual delineation.

The interpretation of the debris covered region could be subject to considerable error. In general, the human brain could easily follow the subtle illumination and colour changes along the outer boundary of the debris-covered ice. However, this could be difficult in regions of shadow and near the terminus when the tongue is flat. In the latter case, a river starting at the terminus might be well visible in the 543 composite and can be used to fix the terminus of the glacier. In the former case (shadow), knowledge about principal glacier flow could be considered to provide a best first estimate where the lateral glacier boundary is (cf. Paul and Kääb, 2005). In cases where nothing is visible, only a rough first estimate will be made.

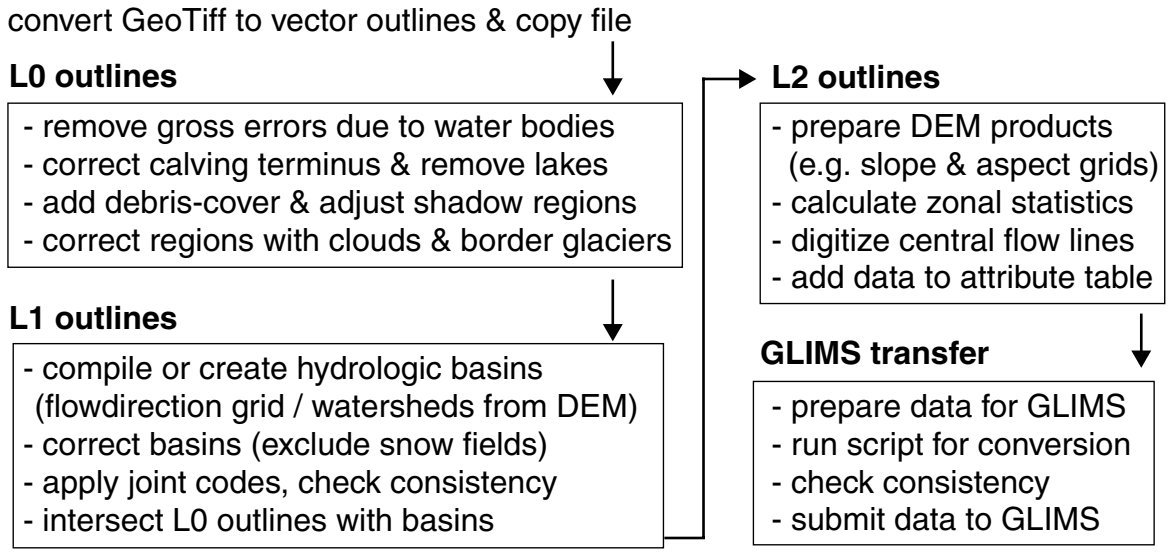

Fig. 4: Workflow of the post-processing steps for glacier mapping and GLIMS transfer.

2.1 Glacier outlines

In some regions it might be difficult to discern debris-covered glaciers from rock glaciers. As rock glaciers will not be included in the inventory, it is intended to apply further criteria for their identification in such cases. This could include, among others: remaining snow fields surrounding the ice body, missing glacier forefields, characteristic surface patterns (lava flow like), typical environmental characteristics, size, etc.

The thresholds for the glacier mapping are selected to optimize the mapping in regions of cast shadow. In this respect, only few corrections should be required here. However, due to specific atmospheric conditions (e.g. thin clouds), crevasses or a polluted bare ice surface it could be possible that manual corrections are required. For this purpose all outlines will be compared to the contrast enhanced band 321 composite and adjusted where visual interpretation allows a clear improvement of the automatically derived outline.

A final issue that has to be considered for the L0 outline product are (optically thick) clouds. There are two major possibilities to use a scene which is partly cloud covered over glaciers nevertheless. One is mosaicing it with multi-temporal scenes, the other is the application of glaciological knowledge. The latter is mainly applicable when only small parts of a glacier are cloud covered so that the outline can be reconstructed. For small clouds located in the accumulation area the assumption that ice is underneath will be reasonable in most cases. This could also be controlled by comparison with scenes from another date. When larger parts of a scene are completely cloud covered (but the scene has favourable mapping conditions in large other parts) the former regions are excluded and replaced by the glacier map from a neighbouring scene (where possible). Within the GLIMS database such a selective processing is supported, as the analyst has to provide an outline (polygon) which encloses the analysed glaciers.

In principal, each glacier outline is controlled by visual inspection and thus validated. In particular glaciers covered by debris are matched against the ground truth provided by the satellite image. Improvement of mapping accuracy is thus mainly expected from scenes with better mapping conditions (regarding shadow and snow) rather than higher resolution satellite imagery or aerial photography, in particular when they have similar or more worse snow conditioons. Regarding debris cover, such higher resolution data might help to better identify the boundary of the glacier or its terminus. However, often the problem is only transferred to the higher resolution as the boundary remains hidden and even in the field it could be difficult to determine its position. Within GlobGlacier, higher resolution data will thus be used as demonstration examples rather than for validation purposes.

Level 1 outlines (L1)
While the L0 outlines depict all regions covered by ice and snow without separating contiguous ice masses, the level 1 product is related to individual glacier entities. Hence, the L0 outlines have to be separated according to the drainage basin of each unit. The points to be considered for defining glacier entities are summarized in Raup and Khalsa (2007). The idea is that the analyst should make a first best estimate of the tributaries that belong to a specific glacier; possible refinements could be applied later. Within GlobGlacier, the glacier basins are

2.1 Glacier outlines

digitized in a separate vector layer as proposed by Paul et al. (2002). This has the advantage that the same basin layer could be applied to different (orthorectified) satellite scenes and in all cases the same entities are extracted. The basin layer has two additional purposes: It is used to make a selection of glaciers (e.g. where snow conditions within a scene are appropriate) and to exclude misclassified snow fields from the glacier area (e.g. lateral avalanche deposits). The resulting basin should only include the glacier parts which are later counted together. All basins are digitized as closed polygons for later intersection with the glacier map. While the points defining the basins could be rough in the ablation region (at least when snow fields are absent), the digitization has to be much more careful in the accumulation region.

From a practical point of view, the ice divide mapping could also be separated into a methodological and a technical part (cf. Racoviteanu et al., in press). For the latter, the basic question is whether a DEM is available or not. When a DEM is missing, a best guess of the location is made based on illumination differences in the 432 composite image and glaciological knowledge about glacier flow. Uncertain divides in the accumulation region are indicated by straight lines (cf. Paul and Kääb, 2005) and a lower positional accuracy could be given for the respective line segment in the metadata table of the GLIMS database. When a DEM is available, the first step is the calculation of a flow-direction grid that allows to delineate divides manually. A second step that will only partly be tested in GlobGlacier is the calculation of watersheds or up-slope area from given seeding points. A related algorithm has been proposed by Schiefer et al. (2008) and will be tested by the GLIMS consortium.

Apart from the technical possibilities on ice divide delineation, some methodological aspects have to be considered as well. The location of the ice divide depends largely on the available data and the glacier type (e.g. ice caps of varying complexity). Four differentiations are made:

a) When a former glacier inventory does already exist and a comparison with former glacier extents is envisaged, the divides are placed at the same locations as in the former inventory (Paul, 2007). When they are not digitally available but have to be derived from printed (sketch) maps, a larger error has to be taken into account. For many regions in the world, glacier locations are available from the WGI. Where they have a sufficient accuracy (four digits behind the dot), they could be converted to the projection of the image and used as an overlay. While this helps to identify individual units, in most cases the location of ice divides is not getting clearer.

b) When no former inventory is available, glaciers are divided in a hydrological sense following the UNESCO guidelines (Müller et al., 1977). In special cases or when a glacier is more shaped like an icecap, the hydrologic divisions are replaced by glaciologic divisions. This could mean that individual units which drain in different catchments on a local scale are not separated but the entire complex is treated as one unit. In some cases the flowfields obtained in WP5 will be used to identify glacier units.

c) Special cases occur where (outlet) glaciers (e.g. draining an ice cap) converge with much larger icestreams (e.g. from the Greenland Icesheet or huge icecaps or icefields) but do not or only partly contribute to the larger unit. The rule here is that such units will be separated from

the larger entity when it is possible (e.g. by well defined medial moraines) and when it makes sense. Hence, such cases will be analysed individually.

d) For a first inventory in a region without further information (DEM, hydrologic basins) the glacier basins are digitized based on the 432 composite image. For later change assessment, it is useful to consider possible larger glacier extents already from the beginning. Hence, trimlines or pro-glacial lakes indicating a former Little Ice Age (LIA) extent should be included in the drainage basin (Paul and Kääb, 2005).

The basins are also used to transfer a common code to all units that once formed the larger entity. This is helpful when changes are calculated as glacier areas can be easily summed up based on their common code (Paul, 2007). A further use of the basins is to select a sub-sample of glaciers from the entire sample. This allows to exclude uncertain classifications (e.g. due to complete snow coverage or debris cover) and incomplete glaciers (e.g. near the image boundary). Digital combination `of` the basins with the glacier outlines will create the individual glaciers that serve as an input for L2 products.

Level 2 outlines (L2)
Level 1 glacier outlines combined with DEM information allow to derive topographic glacier parameters for each unit under consideration (cf. Paul et al., 2002; Kääb et al., 2002; Paul, 2007). The basic principle follows four steps (see Fig. 4):

(1) glacier outlines are converted back to a raster format where each raster cell has the identification code from its respective glacier. So all cells comprising a glacier unit have the same code and form a zone. This step is not required in some GIS software (e.g. ArcGIS) that works directly with the vector outlines (shape files).
(2) Zonal statistics are calculated for each zone (i.e. glacier entity) from an underlying value grid (e.g. a DEM). This gives, for instance, minimum, maximum and mean elevation for each glacier.
(3) Central flowlines are digitized to determine glacier length by intersection with its outline.
(4) The resulting attribute table is joined with the one from the glacier polygons using the glacier code as an identifier. In this way each glacier receives its topographic parameters.

For practical reasons, one zonal glacier grid is created with a zero value for everything that is a glacier and a ‘no data’ entry for all other regions. This zero-glacier grid is different from the original classified map as it only includes the sample of glaciers that should be considered. The main purpose is to restrict calculations to the regions within glaciers and transfer the ‘no data’ flag of rock outcrops and other enclosed non-glacier polygons to the zonal map with the glacier labels. During export of the initial zonal grid, the coordinates of the bounding box and the cell size should match those of the DEM.

Apart from the DEM, other value grids are used to derive further parameters for each glacier: This includes grids describing slope and aspect (its sine and cosine), or a DEM in 100 m steps for calculation of glacier hypsography. The hypsography (area from each glacier per elevation

interval) is calculated by looping over all elevation intervals. A small Fortran program sorts the resulting table from elevation interval -> all glacier IDs, to glacier ID -> all elevation intervals. The mean aspect has to be calculated as the arc tangent from the respective mean values of the sine and cosine grids. The conversion is implemented in a small Fortran program and can be easily adapted to other software. The program also calculates a mean aspect sector for the eight cardinal directions (for scripts see Appendix in Paul, 2007). Mean glacier elevation is calculated by dividing the sum of minimum and maximum elevation by two. In Table 1 all parameters that are calculated from the DEM are summarized.

Nr	Parameter	Symbol	Abbreviation	Calculation
1	Minimum elevation	h_{min}	ele_min	zonalstats
2	Maximum elevation	h_{max}	ele_max	zonalstats
3	Mean elevation	h_{mean}	ele_mean	zonalstats
4	Median elevation	h_{medi}	ele_medi	zonalstats
5	Mean slope	α_{DTM}	slp_dtm	zonalstats
6	Mean aspect (0-360)	ϕ_{deg}	asp_deg	zonalstats+fortran
7	Mean aspect (sector)	ϕ_{sec}	asp_sec	zonalstats+fortran
8	Hypsography (100 m)	-	hypso	zonalstats+fortran

Table 1: Overview of the calculated topographic parameters and abbreviations.

Another important parameter that is derived with the help of the DEM is the central flowline to determine glacier length. While the DEM is used to derive contour lines (e.g. at 50 m equidistance), the connection of the highest and lowest point in the middle of a glacier forms the central flowline. The flowlines are manually digitized (crossing contour lines perpendicular) as automated methods like the steepest downward gradient generally fail in the ablation region with its concave curvature. In principle, it is possible to derive changes in length by intersecting the digitized flowline with the respective glacier outlines. However, in regions of rapid glacier downwasting and retreat like in the Alps, this method fails due to non-uniform geometric changes like emerging rock outcrops in the middle of a glacier (cf. Paul, 2007). Length changes are thus derived by measuring the distance between two terminus positions (see 2.2).

2.2 Glacier terminus position

The terminus position is a point at the glacier front that is used to assess changes in glacier length. It has thus coordinates, a glacier ID and a time stamp. In general, all glaciers that are processed to L1 with a clearly identifiable terminus will receive a point marking the terminus. In cases where the glacier front is more elongated, the intersection of the central flowline with the terminus segment gives the point defining the terminus position. However, for a huge number of (mostly small) glaciers the terminus position will not be defined. On the other hand, poor glacier mapping conditions on former images (e.g. due to seasonal snow) might not allow

2.2 Glacier terminus position

to map the entire glacier accurately, but to identify terminus positions for several glaciers (Svoboda and Paul, in press). In such cases, time series of changes in terminus position (length changes) will be derived. For several regions glacier terminus position will be mapped at four points in time: LIA, 1970s (MSS), 1980/90s (TM), and around the year 2000 (TM/ETM+).

Changes in glacier length (Tier 4 of GTN-G) are determined each year for several hundred glaciers in nearly all parts of the world in the field (e.g. WGMS, 2008). The applied methods cover a wide range and include simple techniques like tape measurements from fixed points in the glacier forefield or portable distance meters (like binoculars) to more demanding theodolite or GPS surveys. Moreover, remote sensing systems (aerial, satellite) are increasingly used (e.g. Li et al., 1998). Due to the complex structure of most glacier termini, several lines of sight are used and averaged for calculation of the change (Fig. 5a). This implies that length changes for a specific glacier tongue could strongly differ when different lines of sight are applied. For this reason a direct comparison of satellite derived length changes with field measurements (e.g. for validation purposes) must be performed with care. However, for longer time periods (e.g. > 10 years) the differences among the individual methods will decrease. (cf. Hall et al., 2003). On centennial time scales (e.g. LIA to 2000) other problems like the split of tributaries occur (Fig. 5b). When it is not possible to determine the former contribution of the tributaries to the main flow, length changes are difficult to determine with confidence. In GlobGlacier such doubtful cases will be excluded.

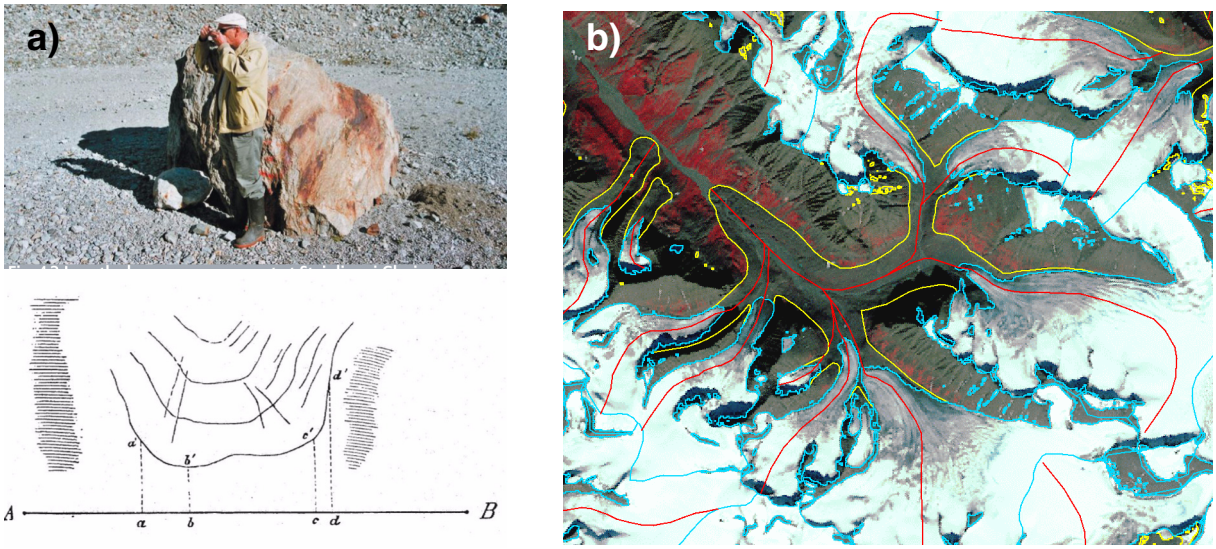

Fig. 5: a) Length change measurements in the field from a fixed point (top) and lines of sight used to determine a mean change (bottom. b) Central flowlines (red) for a formerly compound valley glacier (yellow) on Disko Island (Greenland) that has now split into several branches (light blue). Length changes are derived by intersecting the flowlines with the outlines. The terminal points of the individual branches are rather uncertain in this case.

2.3 Late Summer Snow Line (LSSL) and Snow/Ice Area (LSSIA) retrieval

2.3.1 General concept

The applied algorithm is based on optical satellite data that are used to produce maps of Late Summer Snow/Ice Area Extent (LSSIA) and the Late Summer Snow Line (LSSL). The basic products are maps of snow and ice areas which are used to obtain also the LSSL. As an input accurately orthorectified satellite data in UTM projection (from WP1) and digital elevation data (from WP3) are used. Maps of topographically corrected planetary reflectance or surface reflectance are produced to process LSSIA maps and retrieve the LSSL, using an reflectance threshold for segmentation of snow and ice areas. Where available, field measurements are used to validate results. An optional algorithm during the validation phase applies the full radiative transfer solution to retrieve the surface albedo as a basis for segmentation of snow and ice areas; in this case an estimate or observation of atmospheric properties is needed as an input to the radiative transfer model. Figure 6 shows a general overview on LSSIA and LSSL retrieval from satellite data.

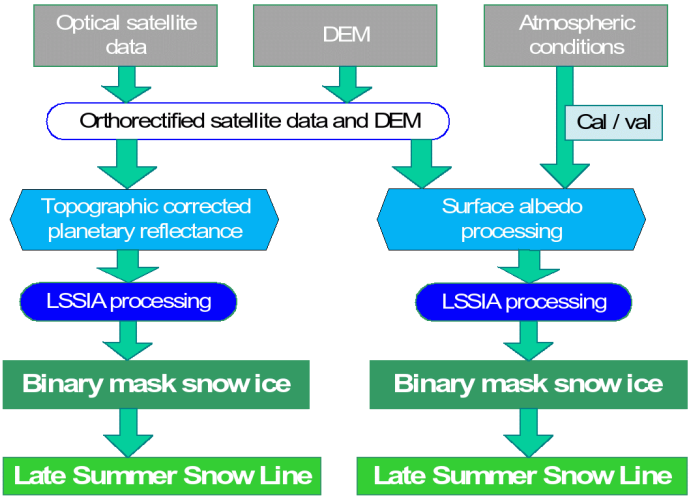

Fig. 6: Overview of Late Summer Snow Line (LSSL) generation. To the left: standard processing line, to the right: processing used for cal/val purposes.

On Alpine mountain glaciers the Late Summer Snow Line (LSSL) corresponds on the average closely to the equilibrium line (EL), the boundary between the ablation area (ice and firn area) and the accumulation area (snow accumulated during the previous winter). The ratio of accumulation to the entire glacier area (AAR) and/or the altitude of the equilibrium line (ELA) are often used as proxy for estimating the mass balance of a glacier (Oerlemans, 2001). This requires knowledge of the mass balance gradients or of empirical relations between AAR and/or the ELA which varies from region to region (Braithwaite, 1984; Chinn et al., 2005).

2.3 Late Summer Snow Line (LSSL) and Snow/Ice Area (LSSIA) retrieval

In the Alps the annual glacier mass balance is usually determined for fixed dates, from 1 October to 30 September of the next year. If the boundary between snow and ice areas is a distinct line, the altitude of the LSSL (or inferred ELA) can be determined by matching a map with the LSSL and topographic data. However, in years of negative mass balance this boundary may be very complicated and the accumulation area could be very patchy (Rott and Markl, 1989). In this case the elevation of the LSSL (or inferred ELA) is a parameter derived from the area-altitude curve taking into account the size of the accumulation and ablation area. For this reason also raster maps of the Late Summer Snow/Ice Area Extent (LSSIA) are produced as a basic product in order to avoid the problem of patchy 'lines'. Such a product offers additional information of glaciological relevance, and is also the basis for retrieving the LSSL.

On high latitude glaciers the identification of the EL and ELA is further complicated by the presence of extended zones of superimposed ice. This is ice which is produced by meltwater from winter snow that percolates through the snowpack and freezes on the ice surface. Superimposed ice belongs to the accumulation zone, but is very difficult to discriminate from ice surfaces by means of its spectral properties as seen by satellite imagery.

For mapping of LSSIA and LSSL (and inferring the AAR and ELA) the time of the satellite image acquisition is important. The image date should be as close as possible to the maximum extent of the ablation area (the end of the ablation period). This is not easy to achieve in many cases, because snowfall events and clouds may obscure the snow line in late summer. An option to minimize this risk is using time series of satellite images through summer. However, major criteria for the scenes selected in WP1 are cloud free conditions and as little seasonal snow as possible. This will also satisfy the demands of WP2.

2.3.2 Basic method for generation of maps for LSSIA and LSSL

Retrieval of snow line and glacier zones using optical satellite imagery

In optical imagery, the LSSIA and LSSL can be identified due to differences in surface reflectance. Glacier ice usually has a lower reflectance than snow. However, snow sometimes has rather low reflectance as well due to pollution by dust and soot or organic material. In these cases the division between snow and clean ice could be difficult. The separation between firn (or névé, which belongs to the ablation area) and snow of the current year could also be difficult because reflectance is often rather similar (Rott and Markl, 1989). Time series of images acquired near the end of summer may be helpful to identify its uppermost position. However, the 16 day repeat cycle of Landsat and frequent cloud cover might only provide a rough estimate. In addition, linear features and texture can be useful for identifying the LSSL in high resolution images.

For automated or semi-automated mapping of LSSIA and LSSL in multi-spectral satellite imagery it is necessary to eliminate the local variations in solar illumination related to topography in order to retrieve reflectance maps. The use of the spectral ratio visible/SWIR(1.6 µm), applied either as a simple ratio or the often used normalized difference snow index (NDSI) does not really help, because the spectral ratio of ice and metamorphic snow is very similar.

2.3 Late Summer Snow Line (LSSL) and Snow/Ice Area (LSSIA) retrieval

An option to discriminate ice, firn, and snow is segmentation based on the surface albedo $R_S(\lambda)$ in one or several spectral channels. In order to derive R_S from satellite data, a high accuracy DEM and numerical model for calculating atmospheric radiative transfer in complex terrain is needed (Nagler, 1996). As an input to the radiative transfer model, information on atmospheric extinction (aerosol content) and scattering properties is needed. They can be taken from available observations or estimated from a data base of typical aerosol types. The calculation of surface albedo is computationally intensive.

A simple option for analyzing large data sets is geometrically (cosine) corrected top-of-atmosphere (TOA) reflectance, RTOA, to be used as a basis for segmentation of snow and ice areas. However, effects of atmospheric scattering may result in significant local differences between cosine-corrected RTOA and the surface reflectance R_S, which may reduce the quality of the snow/ice maps in steep terrain. Because the spectral at-surface irradiance changes with slope and aspect angle (due to different contributions of direct and solar irradiance), good results for reflectance-based classification can only be achieved if radiometric corrections for atmospheric effects are also taken into account. Successful applications for geometry-based parametric corrections of atmospheric influence in mountain areas have been reported for the Minnaert correction and C-correction (Itten and Mayer, 1993). These methods have also been selected as a basic approach for LSSIA and LSSL mapping in this WP.

The segmentation of ice, firn and snow in reflectance maps requires the definition of thresholds for separating these classes. Typical values for the thresholds can be established by comparison of satellite imagery and field data in the context of calibration/validation (cal/val) activities. However, the thresholds may vary spatially and also temporally, depending on the pollution of snow and ice. Therefore, it is mandatory to check the applicability of the thresholds for each satellite image and, if required, use anchor points or image statistics to re-define the thresholds.

Satellite data used for LSSIA and LSSL mapping
The main data base for LSSIA and LSSL retrieval are optical satellite data, as available from Landsat (5 TM, 7 ETM+), ASTER, SPOT (1-5) and Ikonos. In Phase 1 of the project, data of Landsat 5 TM and Landsat 7 ETM+ are used for testing purposes, due to the availability of well orthorectified satellite data, high resolution DEMs, available glacier outlines and field measurements for validation. The software extension for the other optical sensors will be implemented as soon as relevant data sets of those sensors are processed.

To discriminate glacier surfaces from other surfaces in Landsat images the combinations of bands 5, 4, 3 are commonly used, which cover the mid infrared, near infrared and red spectral range. With this combination, snow and ice (in light blue) can be well discriminated from clouds (white), which have a high reflectivity in all 3 bands, whereas the reflectivity of snow and ice is very low in band 5.

The retrieval of snow and ice area maps on glaciers (used also as basis for LSSL retrieval) is based on topographically corrected reflectance. For Landsat 5 TM and Landsat 7 ETM+ the

near infrared band 4 (0.76 - 0.90 m) is the first choice. Bands 1-3 (visible spectral range: 0.45-0.69 µm) are not useful for deriving reflectance maps because of frequent saturation of the signal over snow areas. Bands 5 and 7 in the shortwave infrared spectrum (1.55-1.75 µm and 2.08-2.35 µm) are not useful because of the very low reflectance of snow and ice, and the emitted radiance in band 6 in the thermal infrared (10.4-12.5 µm) does not enable clear discrimination of snow and ice from equally cold regions. For other satellite sensors different spectral bands may be used (e.g. in the visible part of the spectrum) if they are not saturated. An overview of the spectral ranges of the sensors in each band is listed in Table 2. While ASTER and SPOT has no band in the blue range of the spectrum, Ikonos and Quickbird have no SWIR bands.

range	TM		ETM+		ASTER		SPOT 1-5	Ikonos	Quickbird
blue	1	0.45-0.52	1	0.45-0.515		-	-	0.445-0.516	0.45-0.52
green	2	0.52-0.60	2	0.525-0.605	1	0.52-0.60	0.50-0.59	0.506-0.595	0.52-0.60
red	3	0.63-0.69	3	0.63-0.69	2	0.63-0.69	0.61-0.68	0.632-0.698	0.63-0.69
NIR	4	0.76-0.90	4	0.78-0.90	3N/B	0.78-0.86	0.78-0.89	0.757-0.853	0.76-0.90
SWIR	5	1.55-1.75	5	1.55-1.75	4	1.60-1.70	*4/5:* 1.58-1.75	-	-
SWIR	7	2.08-2.35	7	2.09-2.35	5-9	2.145-2.43	-	-	-
TIR	6	10.4-12.5	6	10.4-12.5	10-14	5 bands	-	-	-
Pan		-	8	0.52-0.90		-	*1-3:* 0.50-0.73	0.45-0.9	0.45-0.90
							4: 0.61-0.68		
							5: 0.48-0.71		

Table 2: Spectral ranges of optical sensors: TM (Landsat 4/5), ETM+ (Landsat 7), ASTER (Terra), SPOT 1-5, Ikonos, and Qiuckbird. For the Landsat and ASTER sensors also band numbers are given. The 5 ASTER thermal bands are not shown. The numbers in front of the SPOT spectral ranges refer to the satellite number. Abbreviations: NIR=near infrared, SWIR=shortwave infrared, TIR = thermal infrared, N/B=nadir/back looking. In GlobGlacier mainly the grey shaded spectral bands are used.

2.3.3 Production of reflectance maps

In mountain regions topographic effects of illumination geometry, such as shadowing effects, need to be compensated for calculations that are based on reflectance differences. Two options for compensating topographic illuminations effects were considered in order to retrieve reflectance maps for segmentation of snow and ice areas:

- Calculation of surface albedo by applying an atmospheric radiative transfer model
- Parametric correction of top-of-atmosphere (TOA) reflectance

Option 1 is computationally intensive and requires auxiliary data on atmospheric properties. Therefore this option is used in the project only for cal/val activities. Option 2 is proposed as baseline for retrieval of LSSIA and LSSL maps.

2.3 Late Summer Snow Line (LSSL) and Snow/Ice Area (LSSIA) retrieval

Retrieval of surface albedo

The retrieval of surface albedo is based on numerical solutions of radiative transfer in the atmosphere, including second order scattering effects and surface/atmosphere fluxes. For this purpose we apply the Model 6S (Second Simulation of the Satellite Signal in the Solar Spectrum) (Vermote et al., 1997) which was developed at the University of Lille. We apply an updated version of the 6S Model, developed by the MODIS atmospheric correction group at the University of Maryland in collaboration with the NASA Goddard Space Flight Center. The public domain computer code and documentation are available at http://modis-sr.ltdri.org/6S_code/index.html. Figure 7 shows the concept of atmospheric correction with 6S with relevant details.

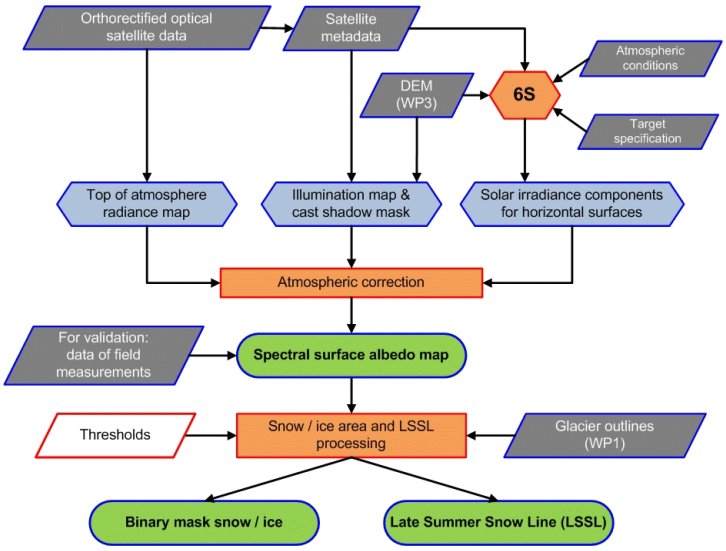

Fig. 7: Atmospheric correction using the 6S model (Vermote et al., 1997).

Sensor parameters of optical satellite data are required as an input. For the most common satellites and sensors the sensor specifications are predefined and can easily be selected. It is also possible to select user defined conditions for a satellite and/or a sensor. The geographic location of a point of interest is ingested in latitude/longitude format. Elevation can be defined manually or derived from a digital elevation model. Several standard atmospheric models are predefined, as well as a selection of standard models for aerosols with option for aerosol type, concentration or visibility, respectively. The atmospheric profiles defined by temperature, ground pressure and relative humidity. A first guess of surface albedo is required which could be defined as global value or as local value. The model allows also the definition of surfaces which are non-Lambertian in their reflectance characteristics.

Based on these input data, the 6S model calculates several parameters, a subset of which is needed for atmospheric correction. The model output includes target reflectance, apparent reflectance and upwelling radiance at satellite altitude, and surface-level irradiance. For valida-

2.3 Late Summer Snow Line (LSSL) and Snow/Ice Area (LSSIA) retrieval

tion purposes, spectral surface albedo will be generated from satellite data, and impacts of uncertainty factors, as impurities of snow/ice, atmospheric effects, and hemispheric directional reflectance (BRDF), will be estimated for specific conditions on single glaciers. For determination of late summer snow and ice, topographically corrected top of atmosphere reflectance is the baseline version. Impacts of the various factors mentioned above will be investigated for this parametrization.

Retrieval of topographically corrected TOA reflectance

Various options for correcting effects of surface topography in the top-of-atmosphere (TOA) reflectance were considered, including correction of geometric effects only, as well as including also parametric corrections of atmospheric effects. Figure 8 shows a flowchart for the retrieval of a topographically corrected planetary reflectance map.

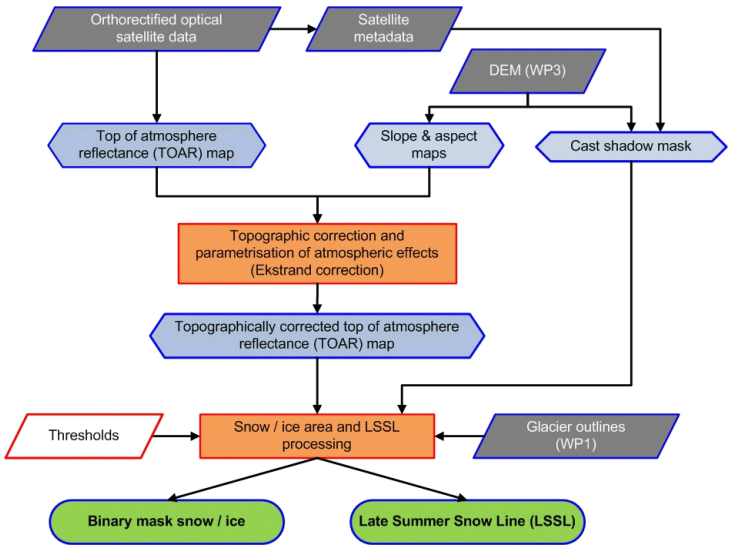

Fig. 8: Workflow for topographic correction of satellite data to derive planetary reflectance.

The following methods were tested:

- *Cosine:* $L_h = L_t * cos(sz) / cos(i)$ *[Eq. 1]*
- *C-Factor:* $L_h = L_t * [(cos(sz) + C) / (cos(i) + C)]$ *[Eq. 2]*
- *Minnaert:* $L_h = L_t * (cos(sz) / cos(i))^{k}$ *[Eq. 3]*
- *Ekstrand:* $L_h = L_t * (cos(sz) / cos(i))^{k * cos(i)}$ *[Eq. 4]*

L_t = radiance on an inclined surface
L_h = equivalent radiance on a horizontal surface
sz = solar zenith angle
i = solar illumination angle in relation to a normal on a pixel
k = Minnaert constant ($0.0 < k < 1.0$)
C = C-factor for modelling diffuse sky radiation

2.3 Late Summer Snow Line (LSSL) and Snow/Ice Area (LSSIA) retrieval

For calculating the reflectance the topographic correction are applied to radiance. In case of Landsat, digital numbers (DNs) are converted to at-satellite radiance by the following formula:

$$L_\lambda = ((L_{MAX,\lambda} - L_{MIN,\lambda}) / (QCAL_{MAX} - QCAL_{MIN})) * (QCAL - QCAL_{MIN}) + L_{MIN,\lambda} \quad [Eq. 5]$$

L_λ = spectral radiance at the sensor's aperture in W/(m^2 sr µm)
$L_{MAX,\lambda}$ = spectral radiance that is scaled to QCALMAX in W/(m^2 sr µm)
$L_{MIN,\lambda}$ = spectral radiance that is scaled to QCALMIN in W/(m^2 sr µm)
QCAL = quantized calibrated pixel value in DN
$QCAL_{MAX}$ = maximum quantized calibrated pixel value (corresp. to $L_{MAX,\lambda}$) in DN (= 255)
$QCAL_{MIN}$ = minimum quantized calibrated pixel value (corresponding to $L_{MIN,\lambda}$) in DN [= 1 (LPGS Products); = 0 (NLAPS Products)]

From the spectral radiance at the satellite, L_λ, the top of atmosphere reflectance can be calculated by:

$$R_t = L_\lambda * \pi * d^2 / E_{sun,\lambda} * cos(sz) \quad [Eq. 6]$$

R_t = Top-of-atmosphere (TOA) reflectance
L_λ = spectral radiance at the sensor's aperture [W/(m^2 sr µm)]
d = sun-earth distance in astronomical units
$E_{sun,\lambda}$ = solar constant at a specific wave length [W/m^2]
sz = solar zenith angle

On the top-of-atmosphere reflectance (R_t), one of the topographic correction methods is applied to obtain the topographically corrected reflectance. The cosine correction is based on the simple ratio of solar zenith angle to incidence angle and results in significant differences to the true surface reflectance because atmospheric effects (e.g. topographic variations in the ratio of direct to diffuse irradiance) are neglected.

The other three corrections account for differences in the atmospheric irradiance by means of empirical factors that are related to changes of the direct/diffuse irradiance and implicitly also for deviations of the surface from the Lambertian (ideally diffuse) reflection behaviour. The Ekstrand correction (Ekstrand, 1996) is based on the Minnaert correction, but weights the Minnaert constant with the cosine of the incidence angle. The correction factors (C-factor, Minnaert constant) can be estimated by means of statistical regression analysis of reflection versus illumination geometry in the satellite image.

After testing all methods, it was obvious that cosine correction is not suitable for topographic correction due to overcorrection resulting in a bias of the reflectance in dependence of local incidence angle. Also the C-Factor correction partly overcorrects the scenes. The Minnaert correction is a suitable method, but especially in steep terrain the Ekstrand correction yields the best results (Fig. A4 in the Appendix). This is also in line with results reported in literature (Law and Nichol, 2004; Törmä and Härmä, 2003; Ekstrand, 1996). Thus, usually the Ekstrand correction (Eq. 4) will be used as a baseline for topographic correction.

2.3.4 Retrieval of LSSIA and LSSL from reflectance images

Maps of surface albedo or topographically corrected TOA reflectance are the basis for retrieving the snow and ice areas on the glaciers by means of segmentation. The reflectance map is combined with glacier outlines of WP1. As explained above, the selection of thresholds is critical for distinguish the various surface types on a glacier. In the broad sense, separation of snow and ice should in general be well feasible. However, the separation between glacier ice (originating by transformation from firn) and superimposed ice (forming by freezing of percolating melt water) is usually not possible. Superimposed ice plays a significant role for mass balance mainly on Arctic glaciers (Wadham and Nuttal, 2002). On the other hand, firn (névé) and snow of the current year can sometimes be well discriminated from snow of the current year (Rott and Markl, 1989). When this is not possible, uncertainties for inferring the AAR and ELA from the satellite derived LSSL results.

The selection of a correct threshold for separating snow and ice areas in the reflectance maps is essential for the quality of the derived products (maps of LSSIA and LSSL). In the first phase of the project, the thresholds will be checked at test sites where field data are available. These data will then be compared with published snow and ice albedo data of glaciers to learn about the representativeness. In addition, reflectance statistics (histograms of reflectance) for glacier areas will be used for individual images to check the setting of the thresholds. For estimating the elevation of the snow line (or inferred ELA) the LSSIAS and LSSL products will be linked with digital elevation data (see Fig. A5 in the Appendix).

For the test site Jotunheimen/Breheimen (Norway) and the Landsat 5 TM sensor, a Minnaert corrected band 4 with a threshold of 0.52 was used to classify the snow. In order to consider also the névé, a slightly lower threshold of 0.47 was also tested. Both thresholds yielded a good first guess for each investigated region (see Fig. A5 in the Appendix). For the test site Ötztal Alps, snow and ice areas have been classified with a threshold of 0.44 based on Ekstrand corrected TOA reflectance in band 4 of a Landsat ETM+ scene from Sep 10, 2004 (see Figs. A6 and A7). In this early autumn scene, glaciers were rather dark due to pollution and the threshold is relatively low. Due to the exceptional warm summer in 2003, no névé areas remained on the glaciers. Knap et al. (1999) performed measurements on snow and ice albedo on Morteratsch Glacier (Switzerland) in the spectral ranges of Landsat TM band 2 and TM band 4 with a field radiometer, including time series and spatial variance over the glacier terminus. For dirty ice in TM band 4 values of surface albedo $R_S <= 0.2$ are reported, and for clean ice $R_S <= 0.4$. In case of very clean ice R_S values may exceed 0.4. For snow $R_S >= 0.5$ was measured in TM band 4, with significant seasonal variance. This suggests that thresholds in TM band 4 in the range $0.4 <= R_S <= 0.5$ are suitable as a first guess for LSSIA retrieval, in agreement with observations in the Ötztal. Surface albedo of course can be different to TOA reflectance (R_T).

The following data layers will be produced:
- Top of atmosphere reflectance map, topographically corrected;
- Snow - ice classification (binary maps);
- Late summer snow line vectors as shape file, as far as the LSSL is clearly definable.

2.4 Topography

As a primary source for terrain elevations GlobGlacier relies on the DEM from the SRTM. As a complement or for assessment of other elevation data sets, DEMs from mapping agencies or similar institutions are used. Where SRTM data are not available or not useful, DEMs will be produced from satellite optical stereo, namely using the ASTER sensor, in some cases also the ALOS PRISM sensor or SPOT. The workflows described here mainly refer to the software PCI Geomatica (module: Orthoengine) and ArcGIS.

2.4.1 InSAR DEM creation

Introduction

Synthetic Aperture Radar interferometry (InSAR) uses phase differences in the radar return signal acquired from two or more different positions in space to detect cm-scale changes in the Earth's surface. The techniques have enabled much greater accuracy in measurements of glacier surface elevation (m-scale) and motion (cm-scale). One of the useful aspects of InSAR is the ability to make these precise measurements simultaneously over areas on the order of 10 000 km^2 (Joughin et al., 2000; Madsen and Zebker, 1998). Another advantage of InSAR compared with other techniques is the ability to retrieve motion and elevation data for featureless regions of ice as found in the interior of Greenland and Antarctica (Goldstein et al., 1993; Joughin et al., 1995; Kwok and Fahnestock, 1996), or generally in the accumulation area of glaciers and icecaps when snow covered. Other techniques need surface features such as supraglacial debris or crevasses to measure ice motion (see 2.6.1). Because InSAR uses volume scattering of the radar signal, the prime requirement is that coherence of the scattering volume is maintained between one SAR acquisition and the next. This imposes a practical limit on the time interval between SAR acquisitions used for InSAR studies of ice elevation and motion (typically 3 days or fewer for ERS C-band SAR) due to e.g. fresh snowfall, melting etc.

Utilisation of a 'window' in the atmospheric absorption spectrum means that this active technique can be used irrespective of cloud cover and illumination conditions, unlike optical techniques. Although in situ GPS measurements are generally more accurate than corresponding InSAR measurements, the former are logistically challenging, expensive and extremely sparse in space and time compared with satellite SAR coverage.

InSAR double differencing for DEM generation and ice motion retrieval

By this method, two interferograms are differenced to remove the phase contribution of the displacement field to obtain a topography-only interferogram. This can then be subtracted from the mixed interferograms to separate the displacement fringe patterns from those due to topography. A constraint for this approach is that at least one of the interferograms must have a large enough baseline to enable extraction of elevation data with sufficient accuracy for geocoding (Mohr, 1997). In the absence of any additional information, the underlying assumption of invariant ice flow over the interval between image acquisitions is reasonable for ice-sheet inland regions during winter, and particularly where short temporal baselines of 1 or 3 days can be achieved.

2.4 Topography

Absolute surface elevation can only be retrieved with the use of tie-points of known elevation (Mohr, 1997), or by fitting the data to an existing DEM (Joughin et al., 1996). In addition, errors in the distance between SAR acquisitions used to form the interferogram (baseline) can be minimised by incorporating independent ground-control points (Joughin et al., 1998; Zebker et al., 1994). InSAR retrieval accuracy varies with the quality of the tie-points used and even minor errors in the interferometric baseline can lead to significant long wavelength errors in the InSAR-derived elevation field.

Processing InSAR data is a complex procedure, with the quality of the final product dependent on both the quality of the datasets and the success of each processing step. The following sequence of interferometric processing steps is generally followed to retrieve ice surface elevation and motion from coherent repeat-pass SAR image pair (cf. Fig. A11 in the Appendix):

1. Selection of a suitable pair of SAR images for required product (baseline, dates etc.).
2. Process raw data to Single Look Complex (SLC) data.
3. High accuracy image co-registration (up to 1/8 of pixel).
4. Interferogram generation. This is generally a simple pixel-by-pixel complex multiplication of the 'master' image by the conjugate of the co-registered 'slave' image.
5. Combination of complex interferograms to isolate topographic phase.
6. Removal of flat-Earth fringes. Required because the fringes in an interferogram have a component due to the Earth's curvature.
7. Phase unwrapping, from modulo-2π to absolute phase.
8. Baseline improvement using ground control points.
9. Conversion of phase to ice elevation. This involves a simple pixel-by-pixel scaling to convert the unwrapped phase image to a height map (DEM).
10. Geocoding to transform the image to map projection space.
11. InSAR-derived DEM used to remove topographic phase from mixed interferogram to isolate phase signal from ice motion (see 2.6.2).

Each of these steps is described in more detail below.

Selection of suitable SAR images

Raw data selection is a non-trivial matter, involving a number of criteria including the interferometric baseline and time interval between the pair of SAR acquisitions. ERS-1 and -2 provide a key dataset for InSAR studies of glaciers and ice sheets, in particular the tandem phase of the mission which lasted 9 months from October 1995. During this mission phase, ERS-1 and -2 orbited in nearly identical orbits, separated in time by 1 day. This short repeat interval means that interferograms formed from tandem SAR pairs typically have extremely high phase coherence. For ERS data, the optimal baseline may be taken to be ~150-300m for height recovery and 0-5m for velocity mapping (Joughin et al., 1996).

A number of online software packages have been developed to help the user select suitable data. Two examples are DESCW and more recently, EOLI-SA (available online), both developed by ESA, which enable the user to see the quality of the SAR backscatter image. For some tandem phase acquisitions, it is also possible to access 'quicklook' interferograms.

2.4 Topography

Raw to SLC

Raw SAR data must first be processed to Single Look Complex (SLC) format which contain the signal information in complex number form - the amplitude and phase information are stored as the real and imaginary parts of a complex number. Several software packages are available for raw to SLC processing, e.g. the Modular SAR Processor (MSP) from Gamma. Figure 10 shows a schematic representation of the MSP algorithm.

In practise, precision information regarding the position and velocity of a satellite at a particular time in its orbit is required to reduce baseline errors and maximise the image co-registration and geocoding. Precision orbit state vectors for ERS are available online from the Delft Institute for Earth-oriented Space Research in the Netherlands (Scharroo and Visser, 1998).

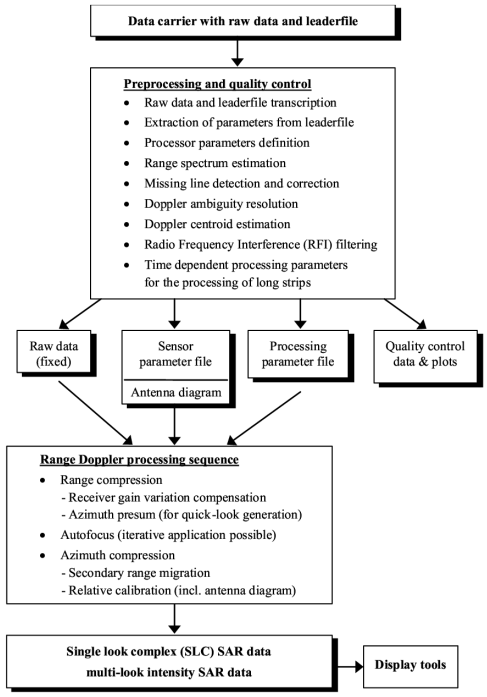

Fig. 10: Algorithm used by Gamma Modular SAR Processor (MSP) to convert raw SAR data to Single Look Complex (SLC) data.

Geometric co-registration

A key initial step in InSAR processing is the co-registration of the input images (both intensity and phase) to a high precision prior to interferogram generation (Gens and Van Genderen, 1996). Co-registration involves the geometric alignment of the 'slave' image to the other reference or 'master' image. Generally, this process entails changing each pixel location in the slave image to match the master image, then interpolating the phase and amplitude information (Gens 1998; Massonet and Feigl, 1998).

2.4 Topography

Accurate co-registration requires a precise knowledge of the offset between the two scenes, such that the secondary can be 'superimposed' onto the master, whilst maintaining the phase content of the pixels. Image offsets occur as a result of uncertainty in sensor location, differences in the look angles between repeat passes and diverging or converging orbits (Kwok and Fahenstock, 1996). Co-registration is generally carried out in 2 stages - the first involves coarse matching to within a few pixels using precision satellite state-vector data (Gens and van Genderen, 1996). Coarse matching is followed by fine co-registration, whereby the image alignment is refined to a fraction of a pixel, typically by comparing roughly corresponding areas and solving for a set of local transformation parameters, either in the frequency or spatial domain (Massonet and Feigl, 1998).

By using Gamma software, two different methods to register the SLC and calculate the interferogram are supported. The first method registers in a first step the second SLC to the reference SLC. Then, the two registered SLC are used for the interferogram calculation. The second method carries out the registration and interferogram calculation in a single step. The first method provides a simple way to register multiple SLC to the same geometry. The main advantages of the second method are the lower disk space used (no additional SLC files are generated) and the higher computational efficiency achieved by the combined application of the interpolation and spectral filtering in one step.

The image registration offsets are modelled as bilinear functions in range and azimuth. Determination of the offset polynomial coefficients is the first step in interferometric processing (Zebker et al., 1994). The co-registration of the images is performed by calculation of the local spatial correlation function for up to a few thousand small areas throughout the image. The image offsets which maximize the local correlation can be determined either by cross correlation of the real valued image intensity or by optimization of the fringe visibility, i.e. using the complex valued signals. These values are used to estimate polynomial coefficients for offsets in both range and azimuth over the whole image. Once the offset functions are known, the two SLC images can be co-registered. As this is done to the sub-pixel resolution, resampling of one of the images is necessary. Appropriate interpolation methods are used to minimize interpolation errors.

Interferogram generation
After co-registration, the complex interferogram is formed by multiplying each complex pixel of the primary image by the complex conjugate of the corresponding pixel in the secondary image. The resulting interferogram contains both the amplitude and phase information. Fringes depicting phase difference at this stage are a measure of the combined surface elevation and displacement in the line of sight of the radar (as well as any errors).

In the interferogram, a phase shift of one wavelength (5.6 cm for ERS) correspond to half a wavelength range displacement (arising from the two-way journey of the radar signal). Assuming no or minimal surface relief (or near-zero baseline), each fringe can be converted to a relative horizontal surface displacement of $2.8/(\delta T \sin\theta)\ \pi$ cm per day in the range direction, where δT is the temporal baseline of the image pair in days and θ is the radar look angle (Gold-

stein et al., 1993; Kwok and Fahnestock, 1996). However, this is rarely the case and topography must be separated from displacement using, for example, interferogram double-differencing (see 2.6.2).

After multiplication, the resultant interferometric phase product is typically multi-looked. By this process, the values of the phase of neighbouring pixels within a fixed window size are averaged. Multi-looking results not only in improved signal to noise ratios (SNR), but also computational efficiency by creating more manageable data. This is an important point, given the size of SAR data acquired at very high spatial resolution, e.g. five-look ERS interferograms. The major disadvantage of multi-looking is that it results in degraded spatial resolution.

Combination of complex interferograms to isolate topographic phase
Phase signal due to topography can be isolated by differencing two complex interferograms, assuming the phase component due to ice motion is identical in the two interferograms. This is usually a valid assumption if the acquisition interval is the same and the acquisition dates are close together and during winter. By differencing the interferograms, the motion phase is cancelled out, leaving topographic phase scaled by the difference in the two interferometric baselines. In the ideal case, long-baseline (typically about 200 m) and short baseline (as small as possible) pairs are differenced, in order to retain high topographic sensitivity (i.e. a large effective baseline) in the resulting topography-only interferogram. With Gamma software, this step is implemented with the routine called *comb_interfs*.

Removal of 'flat-Earth' phase trend
At this stage, it is usually necessary to remove the phase contribution from Earth's curvature. This step is often referred to as 'flattening' and requires precise orbit information (Scharroo and Visser 1998). In Gamma software, the routine *ph_slope_base* calculates the phase ramp to be subtracted by determining the component of the baseline parallel to the look vector for each point across the range swath. Removal of this phase ramp is necessary for accurate estimation of the correlation function, and phase unwrapping. This is especially true for larger interferometric baselines with a large range phase trend. This is because high fringe rates violate the assumption that the phase is constant over the region used to estimate the correlation.

Phase unwrapping
A key issue in SAR interferometry is that the phase information in the interferogram which is related directly to surface topography (Graham, 1974) is only known to 2π (360 degrees of phase). As an example, if one phase cycle represents a 40 m change in height across the image, then it is impossible to differentiate between a height of, for example, 45 m and 85 m in the interferogram since both elevations will have the same phase value (assuming no motion). Consequently, it is necessary to add the correct integer number of phase cycles to each interferometric phase measurement in order to determine the actual elevation at each point. Accurate phase unwrapping is also required for ice sheet velocity interferograms. The process of solving this 2π ambiguity and recovering continuous phase information from the discrete wrapped phase is known as phase unwrapping.

2.4 Topography

The process of phase unwrapping involves searching for the correct integer number of phase cycles that are need to be added to each phase measurement in order to obtain the correct slant range distance. Although a large variety of algorithms have been put forward to solve the phase-unwrapping problem, no consensus has so far been reached as to the optimal approach.

With Gamma software, phase unwrapping is applied using one of two techniques. The first phase unwrapping technique is a branch-cut region growing algorithm and is typically applied to a filtered interferogram. Critical areas such as areas of very low coherence or residues are identified and avoided in the phase unwrapping. The encoded phase unwrapping algorithm is reasonably reliable and requires less computing time to implement.

The second phase unwrapping method uses minimum cost flow techniques and a triangular irregular network (TIN). This technique is a global optimization technique to the phase unwrapping problem. Other advantages of this technique are that gaps in the input data (e.g. at locations of very low coherence) can be considered and the higher density of the TIN. Masking, adaptive thinning, and patch processing, are used to permit efficient and robust unwrapping even of very large interferograms. A more detailed characterization of the phase unwrapping solutions supported by the Gamma software is given by Werner et al. (2002).

Baseline improvement
A first estimate of the interferometric baseline was determined from the orbit data and used to subtract the flat-Earth phase trend. However, this estimate is not accurate enough to convert the unwrapped interferometric phase to topographic heights. Therefore, a refined baseline estimation is performed using a least squares fit for a number of control points of known height. In Gamma software, the *base_ls* routine computes a precise estimate of the interferometric baseline using well distributed ground control points of known x and y image coordinates, the corresponding terrain height, and the corresponding unwrapped interferometric phase. In the absence of an existing DEM it is sometimes possible to extract points of known elevation at the ice margin from high quality maps. For featureless inland ice, airborne or spaceborne altimeter data are typically used.

Phase to height conversion
The Gamma routine *hgt_map* reads the phase unwrapped interferogram and the baseline geometry and reconstructs the terrain height and cross track position for each pixel and on the WGS84 ellipsoid Earth model. The unwrapped phase is a measure of the propagation path length difference between the received signals used to generate the interferogram. This is combined with the baseline data for each line in the image to calculate the look vector from the radar to the point on the ground.

Height map geocoding
At this stage, the geometrically calibrated interferogram is in slant range geometry, i.e., it consists of arrays of pixels fixed into a geometry corresponding to the acquisition parameters of the satellite. For the data to be used quantitatively, they must be geocoded. The process involves assigning pixels within a given image with ground coordinates. The act of geocoding

and subsequent transformation into a map projection puts the image into ground range and creates a raster-based DEM. This enables the co-registration of interferometric results with data from other sources e.g. GPS and airborne laser altimetry and also the correction of radar artefacts such as image foreshortening and layover in regions of steep terrain.

The Gamma routine *gc_insar* calculates a complex valued transformation lookup table for terrain corrected geocoding. The calculation is based on heights in SAR coordinates as retrieved from SAR interferometry. The transformation lookup table describes the geometric transformation between images in SAR (range-Doppler) coordinates and a user selected map projection. The complex valued lookup table has the dimension of the images in the SAR coordinates. Each complex value contains the corresponding map coordinates with the real part related to the real valued column (i.e. easting or longitude) and the imaginary part related to the real valued row number (i.e. northing or latitude). The geocoded height map is output in GeoTif format and if necessary reprojected with GDAL -software to the UTM projection.

2.4.2 SRTM

The 3 arc sec (approx. 90 m) resolution SRTM DEM will be used as the core data set for deriving topgraphic information. This DEM has been created in February 2000 at C-band wavelength from the interferometric techniques described before. Because the C-band can penetrate through dry snow, the DEM refers to the Autumn 1999 surface on the Northern Hemisphere. The (partly huge) data voids which are often observed in steep mountain terrain are generally located just outside of glaciers as they have a more gentle surface (see 2.5.1).

Post-processing

Readily processed SRTM DEM data of version 4 are downloaded from a public website (http://srtm.csi.cgiar.org/) in the size of 5 degree by 5 degree tiles. In this dataset, voids in the original SRTM DEM are interpolated with the interpolated regions marked in a second data set (mask), that is also downloaded. The two SRTM data layers are exchanged in the GeoTif format which can be directly read, cut, or else manipulated in PCI Geomatica, ArcGIS and other remote sensing and GIS software. Each SRTM tile is cut to the size of the study region or is combined from several SRTM tiles when required. The resulting DEM is transformed and projected in the UTM zone of the study region.

The SRTM DEM, the mask of interpolated values, and the overlapping orthoprojected Landsat 5 or 7 scenes are loaded in a GIS and the following assessments are performed:

- Check if substantial glacier areas consist of interpolated values.
- Create SRTM hillshades and visually inspect them for processing and interpolation artifacts.
- Create SRTM contours, overlay them on the Landsat scenes and visually check for errors and artifacts. Indications for SRTM DEM errors are sections where the contour lines do not agree with the topography as visible in the satellite image. Such disagreements can be (1) topographic features depicted in the image but not present in the DEM, (2) topographic features of the DEM that are not visible in the image, and (3) topographic features that have a horizontal offset between the image and the DEM.

- Drape the satellite image over the DEM and check through 3D visualisation or fly-throughs for areas where image and DEM do not correspond.
- If available, parts of the SRTM DEM are compared to other DEMs (see following sections).
- For selected test sites orthoimages of an ASTER nadir channel 3N and an backward channel 3B are computed using the SRTM DEM. For a DEM free of vertical and horizontal errors, the 3N and 3B orthoimages should perfectly overlap. On the other hand, horizontal shifts between the two orthoimages are a clear indication of DEM errors in the respective terrain sections. The underlaying DEM error is estimated from the horizontal shifts at distinct places by dividing the shift through the stereo ratio of the sensor, in case of ASTER about 0.6. (Kääb, 2002 and 2005a). According DEM tests can be performed using ALOS PRISM stereo pairs or triplet images.

From the above assessments a qualitative and, if possible, quantitative description of the accuracy and quality of the SRTM DEM for each study region is compiled and related to the global and average accuracy specifications of the SRTM DEM (Rabus et al., 2003).

2.4.3 DEMs from mapping agencies

Post-processing

DEMs from mapping agencies or similar institutions were commonly compiled directly using aerial photogrammetry or digitized from contour lines that were derived from aerial photogrammetry. The detailed procedures for DEM derivation, however, might vary significantly and are not in all cases well documented. In most cases DEMs from mapping agencies will cover only small sections of study regions. Within GlobGlacier, DEMs available from mapping agencies are converted to GeoTiff so that they can be directly read, cut, or else manipulated in PCI Geomatica, ArcGIS and other remote sensing and GIS software. The DEM is transformed and projected in the UTM zone of the study region.

The DEM, the SRTM DEM (if available) and the overlapping orthoprojected Landsat 5 or 7 scenes are loaded in a GIS and the assessments as described above for SRTM can be performed in the same manner. The most important points are:

- Check the date of the DEM and compare the dates of the other products. Assess potential temporal changes between both products.
- Create DEM hillshades and visually inspect them for artifacts and completeness.
- Create contours, overlay them on the Landsat scenes and visually check for errors and artifacts (see above for further details).

From the above assessments a qualitative and, if possible, quantitative description of the accuracy and quality of the DEM for each sub-region is compiled and related to the general and average accuracy specifications of such DEMs. In most cases, the mapping agency DEM will serve as a validation for the SRTM DEM, and DEMs compiled from satellite optical stereo and SAR interferometry. In some cases, DEMs from mapping agencies might be the only elevation information available to GlobGlacier.

2.4 Topography

For some countries (e.g. Greenland) DEMs are only available in a vector format (e.g. elevation contours, spot elevations, lake outlines, river networks, etc.) or, in the case of Canada, are freely available in this format from the internet (www.geogratis.ca). These data could already be used to assess elevation changes at the position of the contour lines (Kääb, 2008 and example in Fig. A9b) or as an input for generating a (raster) DEMs. Within GlobGlacier, the *topogrid* interpolation as implemented in the Arc/Info GIS will be used for this purpose.

2.4.4 Optical satellite stereo

Satellite optical stereo DEMs are produced from ASTER bands 3N (nadir) and 3B (backward), or ALOS PRISM forward, nadir and backward data (F, N, B). The principle data acquisition scheme for both sensors is illustrated in Fig. 11.

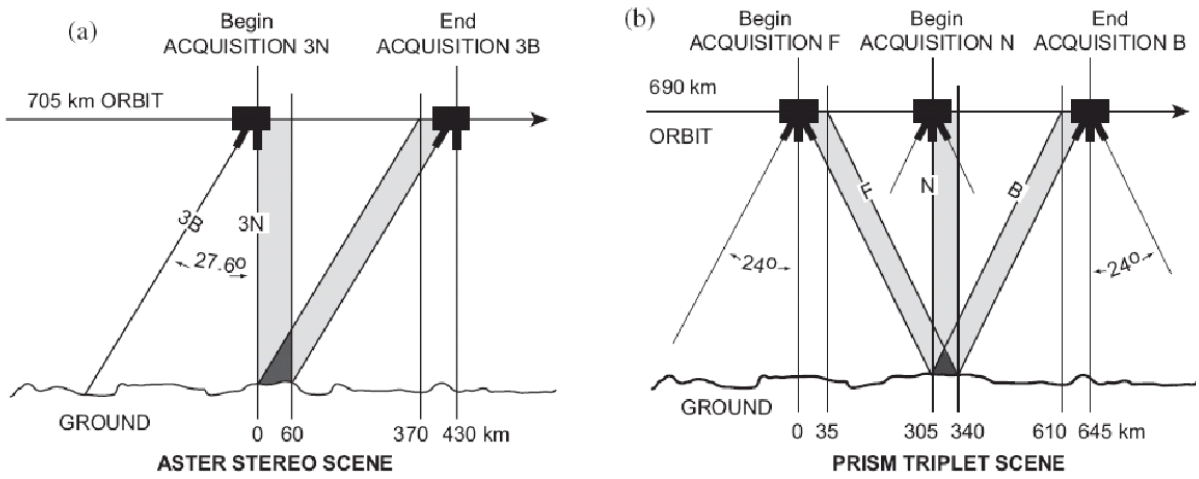

Fig. 11: Geometry of two satellite along-track stereo systems for digital terrain model generation. a) ASTER's nadir channel (3N) and backward-looking channel (3B) form a stereo scene with 15 m spatial resolution. b) The ALOS PRISM sensor has a forward channel in addition to nadir and backward channels. All three form a triplet scene with a nominal 2.5 m resolution.

Scene selection

The criteria for selecting ASTER or ALOS PRISM scenes for DEM generation are:

- Date: close to the date of other data to be combined with the ASTER DEM, or complementing other DEMs in order to construct time series of terrain geometry (see 2.5).
- Terrain and illumination conditions: radiometric contrast is usually maximal for scenes with little (fresh) snow cover, and small shadow areas.
- Sensor settings: radiometric contrast is usually maximal for scenes with sensor gain settings that produce no or only few saturated pixels in the image. Detector saturation is, though, a common problem over snow and in particular fresh snow (see 2.2).

2.4 Topography

Preprocessing
The most important preprocessing step before compiling DEMs from optical stereo is destriping of the images used, or removal of other radiometric or geometric patterns, such as alignment errors of composite array sensors (e.g. ALOS PRISM). These errors would significantly complicate the matching of stereo parallaxes and/or introduce parallax matching errors. Within GlobGlacier, destriped or else corrected data levels (e.g. ASTER 1B, instead of 1A) are used, or these corrections are done automatically during the image import using the calibration parameters contained in the image header. PCI Geomatica for example destripes ASTER level 1A data during the import process using the image header information.

If it turns out during first DEM generations and evaluations that the multiple line array alignment errors of ALOS PRISM are not sufficiently corrected, individual data subsets of single line arrays are used for DEM generation.

Orientation
The parameters of the geometric sensor model of an individual satellite scene have to be known for, among others, DEM generation and orthoprojection of the image. A schematic illustration of the processing steps is depicted in Fig. 12. For this purpose (1) the according satellite navigation data contained in the image header and georeference information can be used, or (2) the sensor model can be solved using ground control points (GCPs). The positional information of ASTER and ALOS PRISM data has variable accuracy, ranging from many to several tens of meters. In general, approach (2) is used in order to achieve optimal co-registration between the ASTER or ALOS PRISM derived products and other data. For this purpose, GCPs will be taken from pre-existing data such as DEMs, their hillshades or orthoprojected Landsat data (panchromatic band). The sensor model implemented in PCI Geomatica Orthoengine requires at least 6 GCPs. Between 10 and 30 are chosen for GlobGlacier products. This provides reliable measures for the georeference accuracy that will be reported.

For selected scenes the accuracy of the satellite navigation data (1) will be tested by comparing it to the image orientation obtained from (2). ASTER on-demand DEMs are also available from NASA, distributed by LPDAAC. These DEMs are produced using the Silcast software, which relies on the orientation approach (1). For selected scenes, such ASTER on-demand DEMs will be ordered in addition and compared to the other DEMs. In phase2 of the project, the global ASTER DEM (also generated by the Silcast software) might become available. When previous tests have proven an acceptable accuracy of the product, we will extensively use it outside the coverage of the SRTM DEM.

DEM generation
Once the sensor model parameters are determined, epipolar images can be produced within the PCI Geomatica Orthoengine software module. Although these are just an intermediate step towards DEM generation, the stereo model by the epipolar image pairs can be viewed in 3D, for example using the anaglyph technique. Gross errors in the image orientation usually become visible as distinct distortions in the stereo model. This visual test is performed for the ASTER scenes and, if necessary, the image orientation improved.

2.4 Topography

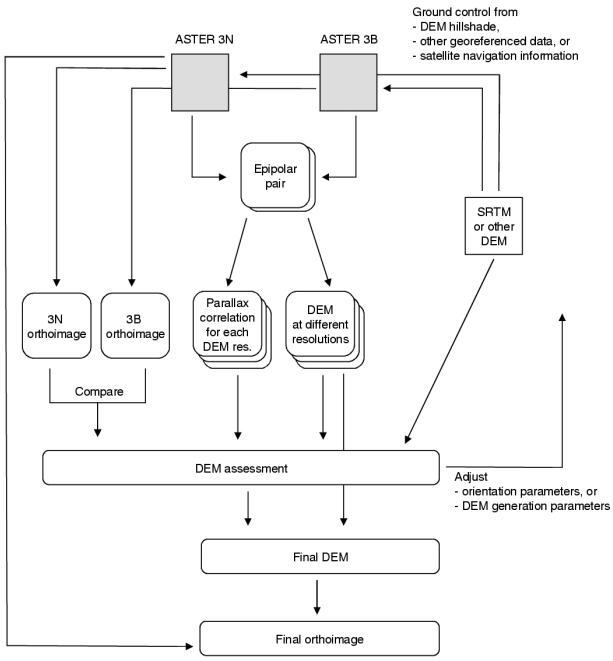

Fig. 12:Flow chart for DEM generation from ASTER satellite stereo including DEM assessment procedures.

From the epipolar pairs the stereo parallaxes are matched and the according DEM is produced using the Orthoengine module. DEM generation is with "high terrain detail" setting. The matching grid resolution is with 2, 4 or 8 pixel resolution (30, 60 or 120 m for ASTER). This setting is chosen individually for each scene depending on the terrain roughness and radiometric contrast in the image. In general, rough terrain with sufficient optical details allows for 2 or 4 pixel DEM matching distance, smooth terrain with less contrast is usually best captured with 4 or 8 pixel resolution. In general, DEMs of all three pixel resolutions are produced together, in uncertain cases all three resolution levels, and compared in the postprocessing stage.

As a special feature of high value for DEM error detection and postprocessing, PCI Geomatica allows for storage of a second DEM layer containing the DEM matching correlation value for each DEM cell. This layer is produced for each ASTER or ALOS PRISM derived DEM.

Orthoimage generation
Using the final DEM, orthoimages are produced from the different stereo channels (3N and 3B; F, N, and B) and an ASTER bands 3, 2, 1 false colour composite. Since these orthoimages are, among others, used for quality assessment of the DEMs, which might as a consequence be improved, orthoimage production might be repeated in an interactive process with the following postprocessing steps.

Post-processing
The following test and, if necessary, improvements are performed for each ASTER or ALOS PRISM derived DEM. They are very similar to the assessments performed for SRTM.

- Check the DEM for voids.
- Create DEM hillshades and visually inspect them for processing artifacts.
- Create DEM contours, overlay them on the orthoimages and visually check for errors and artifacts. Indications for DEM errors are sections where the contour lines do not agree with the topography as visible in the satellite image (see 2.4.2 for an explanation).
- Drape the orthoimage over the DEM and check through 3D visualisation or fly-throughs for areas where image and DEM do not correspond.
- Compare the 2 and 4 pixel, 4 and 8 pixel, or 2, 4 and 8 pixel resolution DEMs by calculating their vertical differences. Differences of several tens to hundreds of meters point to DEM errors (DEM resolution pyramid).
- Analyse the parallax matching correlation layer (so-called score channel) together with the DEM, the orthoimages and the differences from the DEM resolution pyramid. If necessary, formulate using map algebra a rule for excluding certain areas of the DEM, with for instance too low parallax score and too large differences between the DEM resolution pyramid levels.
- If available, parts of the DEM are compared to other DEMs (see above and below).
- Compare the orthoimages of the ASTER nadir channel 3N and the backward channel 3B. For a DEM free of vertical and horizontal errors, the 3N and 3B orthoimages should perfectly overlap. On the other hand, horizontal shifts between the two orthoimages are a clear indication of DEM errors in the respective terrain sections. The underlaying DEM error can be estimated from the horizontal shifts at distinct places by dividing the shift through the stereo ratio of the sensor, in case of ASTER about 0.6. (Kääb, 2002 and 2005a). Corresponding DEM tests can be performed using ALOS PRISM stereo pairs or triplet images.
- As a consequence of the above tests and assessments, the DEM might be recomputed using modified parameters, the final DEM might be combined from different levels of the DEM resolution pyramid, or certain DEM areas might be removed or interpolated.

From the above assessments a qualitative and quantitative description of the accuracy and quality of the satellite optical stereo DEM for each study region is compiled and related to the global and average accuracy specifications from the literature.

SPOT 5 DEM
For some selected Arctic regions DEMs from the SPOT 5 sensor as provided in the framwework of the IPY project SPIRIT will be integrated. In principal, data processing for along-track SPOT 5 stereo data is similar to ASTER and the same accuracy measures apply. Although there will be little control on the accuracy of the SPIRIT DEM product by GlobGlacier, data layers which are useful for quality assessment (correlation values) are included in this product. Where possible, the product will be compared to other DEMs and might even be used for calculation of elevation changes.

2.5 Elevation change

Glacier elevation changes have a close relation to glacier mass balance and can be interpreted as the direct response to the annual atmospheric forcing. A major difference is that mass balance is given in meter water equivalent (m w.e.) which implies that the density of the material (ice, snow, firn) has to be known. Usually this is done in the course of field measurements with the direct glaciological method. However, when longer periods of time are investigated (c. 10 years) it can be assumed that the observed elevation change is due to changes in ice mass and the ice density can be used for conversion. The mass balance as measured for hydrological purposes refers to the actual glacier size and a geodetic calibration of the measured series after c. 10 years for the entire glacier is mandatory to account for systematic or random measurement errors. This has to be considered when satellite-derived values are compared to field data.

Most of the glaciers in the current global monitoring network are small (1-10 km^2) compared to the glaciers and icecaps (> 100 km^2) that really contribute to global sea level rise. In this respect, different techniques are applied to assess their elevation changes: airborne laser profiles or satellite-based point elevation measurements for large glaciers, and field surveys and aerial photography (or laser scanning) for the small glaciers in the network. In WP4 both satellite-based point elevations and satellite-derived DEMs (cf. description of WP3 in Ch. 2.4) will be used in combination with further elevation information (e.g. national DEMs) to assess elevation changes over various periods of time. DEM differencing will directly obtain the elevation changes for an entire glacier while the changes obtained at points have to be extrapolated over the entire glacier surface to get a comparable value. The subtraction of DEMs covering large regions allows to assess the representativity of the glaciers in the mass balance monitoring network for the mass change in entire mountain ranges (Paul and Haeberli, 2008).

2.5.1 DEM subtraction

The sources which can be used for the DEMs are manifold (see 2.4). The selection of DEMs for differencing should consider that their accuracy is better than the expected changes, i.e. the time interval should be larger when the accuracy is reduced. Such zones of reduced accuracy can be found in the accumulation area of glaciers when the DEM is derived from optical imagery (stereo correlation frequently fails over saturated surfaces) or in steep/obscured terrain for microwave/optical sensors. Once an appropriate DEM pair has been selected, the projections/datum and the spatial resolution must be matched. When DEMs of different spatial resolution are compared, elevation changes over stable non-glacier terrain should only be identical in flat regions in order to avoid artefacts due to the differing resolution (Paul, 2008). For example, when the SRTM3 DEM is subtracted from an earlier national DEM (25 m resolution) the reduced elevation in the coarser resolution SRTM3 DEM over steep terrain causes an artificial bias with elevation (cf. Berthier et al., 2006) as mountains usually get steeper towards higher elevations. The radar penetration of the C-band sensor in dry snow (up to 10 m) has also to be considered. A common way to adjust the two DEMs is by minimizing the standard deviation of the difference DEM. This value is very sensitive to positional inaccuracies in steep terrain and becomes easily visible when the difference DEM looks like a shaded relief of the terrain. In this case, the spatial matching is not sufficient and should be further adjusted.

2.5 Elevation change

For normal, glaciers are well visible in differences image from the past decades, as they are the only surfaces with a (more or less) homogenous elevation loss (Fig. 13). For all other regions the picture should be scattered without a bias depending on aspect and elevation. However, at steep slopes the coarser resolution DEM should have lower (convex curvature) or higher (concave curvature) elevations. Systematic differences will also appear when DEMs (or DTMs) are compared to digital surface models (DSMs) which include vegetation or buildings. So regions with forest will be clearly visible in the related difference image. In alpine terrain lakes which are used for hydropower production will also clearly reveal lake level variations between the two acquisition dates or season (e.g. winter for microwave, end of summer for optical DEMs).

When using the SRTM3 DEM for differencing, some care has to be taken for the data voids. Luckily, most glaciers are located just outside the voids (due to their gentle slope and surface) and elevation changes could be assessed for the entire surface (Fig. 13). However, it is recommended to buffer the data voids by one or two pixels (to exclude artefacts near the voids) and to include only glaciers in statistical calculations that are less then 20% covered by data voids. Experiences from DEM differencing in Switzerland using a national DEM from around 1985 and the SRTM DEM from 2000 (cf. Paul and Haeberli, 2008) revealed that a dichromatic colour coding in steps of 1/2 standard deviations is most useful to illustrate the changes (Fig. 13).

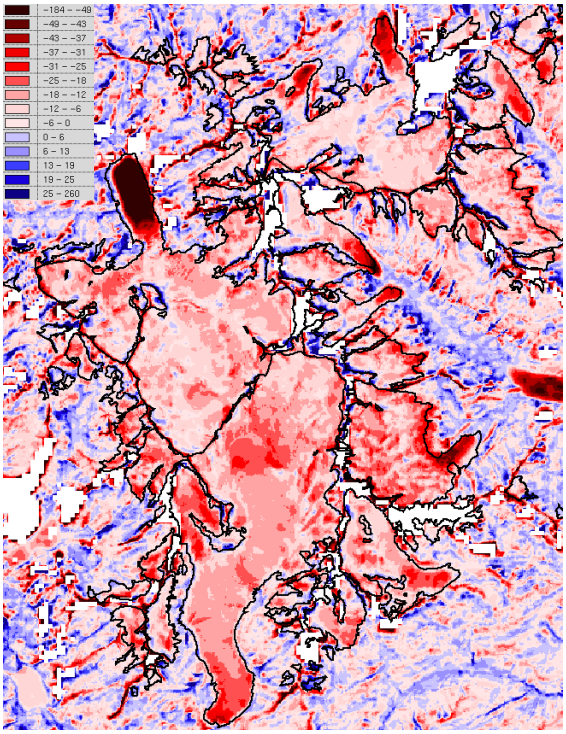

Fig. 13: Result of the DEM differencing with the SRTM3 DEM and the swisstopo DEM25 level 1 for the region around Rhone and Trift glaciers. The strong elevation loss at most glacier tongues is illustrated with remarkable clarity. Black outlines give glacier extent in 1973.

2.5.2 IceSAT GLAS data

Data used for Ice, Cloud, and land Elevation Satellite's (ICESat) Geoscience Laser Altimeter System (GLAS) elevation change product is the GLAS/ICESat L1B Global Elevation Dataset or "GLA06" available free of charge online from the National Snow and Ice Data Center (NSIDC) (Zwally et al., 2003). GLAS is the main instrument of ICESat satellite launched in 2003. The main objective of the ICESat mission is to measure changes in elevation of the Greenland and Antarctic ice sheets (Zwally et al., 2002).

ICESat GLAS is a laser altimeter measuring surface elevation. A footprint of GLAS in the surface of the earth is approximately 60 m and along track spacing between subsequent measurements is approximately 172 m (Zwally et al., 2002). Due to the nature of laser altimeter measurement, surface elevation measurements are possible only under cloud free conditions. ICESat was launched in January 2003 and the GLAS instrument has been operational in 14 operation periods each approximately 35 days long since. Dates of operational periods for which data is available is presented in Table 3. Data from 8-day repeat track orbit is not useful for elevation change product creation and thus only data from 91 day repeat track orbit that the spacecraft was put into in October 2003 is used.

Operation Period	Start Date	End Date	Starting Track	Ending Track
Laser 1	2003-02-20	2003-03-29	8-day #72	8-day #23
Laser 2A	2003-09-25	2003-10-04	8-day #88	8-day #100
Laser 2A	2003-10-04	2003-11-19	91-day #1098	91-day #421
Laser 2B	2004-02-17	2004-03-21	91-day #1284	91-day #421
Laser 2C	2004-05-18	2004-06-21	91-day #1283	91-day #434
Laser 3A	2004-10-03	2004-11-08	91-day #1273	91-day #452
Laser 3B	2005-02-17	2005-03-24	91-day #1258	91-day #426
Laser 3C	2005-05-20	2005-06-23	91-day #1275	91-day #421
Laser 3D	2005-10-21	2005-11-24	91-day #1282	91-day #421
Laser 3E	2006-02-22	2006-03-27	91-day #1283	91-day #424
Laser 3F	2006-05-24	2006-06-26	91-day #1283	91-day #420
Laser 3G	2006-10-25	2006-11-27	91-day #1283	91-day #423
Laser 3H	2007-03-12	2007-04-14	91-day #1279	91-day #426
Laser 3I	2007-10-02	2007-11-05	91-day #1280	91-day #421
Laser 3J	2008-02-17	2008-03-21	91-day #1282	91-day #422

Table 3: ICESat GLAS operation periods.

The NSIDC GLAS Altimetry elevation extractor Tool (NGAT) is used to extract elevation and geoid data from the binary GLA06 altimetry product. Output of NGAT is an ASCII table of record number, time of measurement, latitude, longitude, elevation, geoid, saturation elevation correction and gain value as used for the received pulse. An example of the NGAT output is given in Table 4.

2.5 Elevation change

Record #	Date	Time	Latitude	Longitude	Elevation	Geoid	Range cor.	Gain
235549302	09/30/2003	15:02:11.205	74.858787	273.790028	648.043	0.051538	0.000	126
235549302	09/30/2003	15:02:11.230	74.857301	273.788345	649.033	0.040000	0.000	106
235549312	09/30/2003	15:02:11.255	74.855815	273.786661	644.172	0.030000	0.000	80
235549312	09/30/2003	15:02:11.280	74.854328	273.784977	640.845	0.018462	0.000	58
235549312	09/30/2003	15:02:11.305	74.852839	273.783292	635.880	0.006923	0.000	63

Table 4: Example of NGAT output of IceSAT data.

For elevation change analysis, the NGAT output and glacier outlines are read into Matlab. Elevation values *z(x, t)* inside the outline are plotted, and orbital crossover points are found first by manually giving an initial guess and finally searching the crossovers near every manually input point by fitting a first degree polynomial to ground tracks and arithmetically solving the exact crossover point. The overall elevation change product creation chain is presented in Fig. 14.

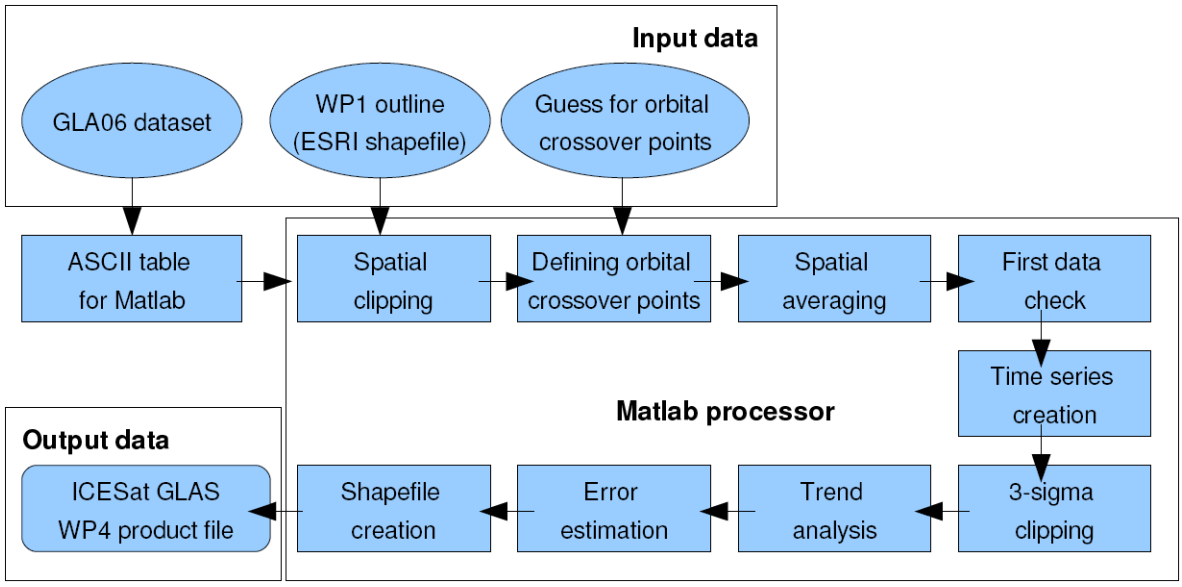

Fig. 14: Flow chart of ICESat GLAS elevation change product creation.

The elevation value $z'(x_C, r, t)$ representing each orbital crossover point at location x_C for each operation period is calculated as an average of elevations with distance of averaging radius r or less from the orbital crossover point. Selection of a suitable r is a compromise between having a large enough area to minimize the error introduced by ground tracks at different times not coinciding and the possibility to include bad elevation measurements into the average. Typical value for r used in processing of GlobGlacier products is between 300 and 500 m. If the surface tilt is small enough, an elevation value can be obtained without any averaging, but by

2.5 Elevation change

interpolating elevation at exact orbital crossover points for both ascending and descending tracks and using an average of the two if their difference is smaller than a given threshold. However crossover points from different years rarely coincide in date and distances between exact crossover points for each operations period can be in the order of hundreds of meters. This approach can thus only be used is surface tilt is less then 0.1% which rarely is the case in ice caps of interest for the project.

Accuracy and precision of GLAS measured elevations has been studied on the Antarctic Icesheet. Accuracy is found to be decreasing with surface slope from about 14 cm at small surface tilts (0-0.25 degrees) to about 25 cm at tilts of 1-2 degrees. Precision of GLAS elevations is estimated to be approximately 2 cm (Shuman et al., 2006). We assume that the accuracy and precision of GLAS on ice caps is of the same magnitude.

Apart from mean elevation $z'(x_C, r, t)$ around the crossover point x_C, also the number of elevation measurements $N(x_C, r, t)$ and standard deviation of elevations $\mathrm{std}(z(x_C, r, t))$ that fall inside a given radius for each crossover point is calculated. Crossover points with too few measurements or too large standard deviation (threshold values N_{th} and σ_{th} respectively) are discarded as bad data in the first data check according to the following equation:

$$if\,(N(x_C,r,t)<N_{th} \vee \underset{|(x_C-x)|\le r}{std}\,(z(x,t))>\sigma_{th}) \Rightarrow discard\,data \qquad [Eq.\ 7]$$

Time series of spatially averaged elevations for each orbital crossover point are then compiled. Mean elevation and standard deviation over time for every crossover position are calculated and elevation values that deviate more than three times the standard deviation from the mean value are discarded from the time series - this known as 3-sigma clipping:

$$if\,z'(x_C,r,t_i) - \underset{i=1,2,3...}{mean}\,(z'(x_C,r,t_i)) > 3\,\sigma(x) \Rightarrow discard\,data \qquad [Eq.\ 8]$$

After the 3-sigma clipping, a first degree polynomial is fitted to the time series of elevations, with slope is representing the elevation trend dz/dt. Error estimates for the elevation trend in point x over the observation period is defined in the following equation.

$$e_{(dz/dt)} = \frac{\underset{i=1,2,3...}{std}\,(z'(x_C,r,t_i))}{max(t)-min(t)} \qquad [Eq.\ 9]$$

The last step of the processing chain is to write output variables including elevation, time, geographical coordinates, elevation trend and error estimate of elevation trend into a product shapefile. Data fields of the WP4 ICESat GLAS elevation change product are presented in Table 5. If the projection of WP1 glacier outline product used is not in geographic coordinates, the ogr software suite will be used to reproject the elevation change product to comply with the WP1 product and the agreed project projection system (which is UTM for internal use).

2.5 Elevation change

Symbol	Explanation	Data type
t	Time (years)	N element vector
z	Mean measured elevation around crossover point at time t	N element vector
dz/dt	Elevation trend [m/y]	Number
e_dz/dt	Estimated error in elevation trend [m/y]	Number
r	Averaging radius used [m]	Number
N	Number of elevation measurements in timeseries	Number
Lat	Latitude of orbital crossover point [degrees]	Number
Lon	Longitude of orbital crossover point [degrees]	Number

Table 5: Data fields of ICESat GLAS elevation change product

2.5.3 Elevation change from Envisat Radio Altimeter 2 (RA2) data

The Radio Altimeter 2 (RA2) is a nadir-looking pulse-limited radar altimeter based on the heritage of ERS-1 RA and functioning at the main nominal frequency of 13.575 GHz (Ku Band) for measuring elevation *h* of the surface below. RA2 is flying with European Space Agency's satellite Envisat launched in March 2002. A schematic overview of the RA-2 processing is given in Fig. 15.

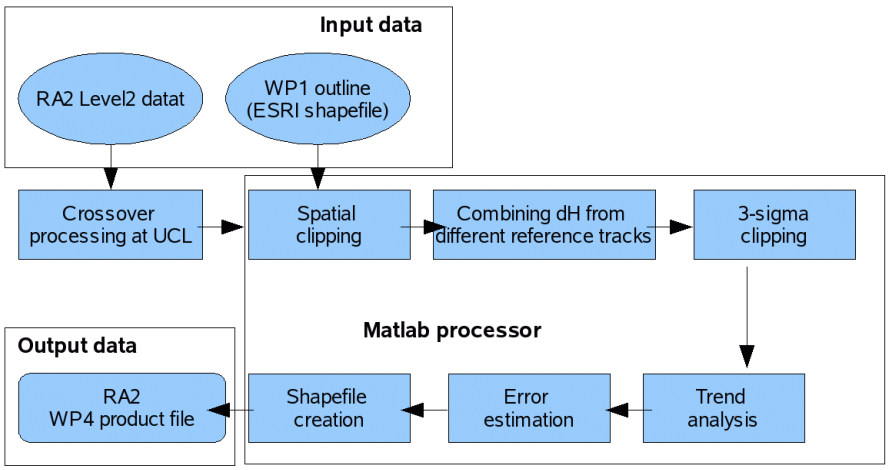

Fig. 15: Flow chart of Envisat RA2 elevation change product creation.

Envisat RA2 data as used for GlobGlacier is processed by University College of London (UCL) Centre for Polar Observation and Modelling from RA2 GDR format Level-2 data. Elevation differences $Dh(x, t_1, t_2)$ are calculated for all orbital crossover points (points where ascending and descending orbit ground tracks meet) on Arctic land areas between 81.5 and 65 °N. The upper latitude limit is constrained by the satellite orbit and the lower one is a chosen processing parameter. Elevation at orbital crossover points is interpolated from two nearest measurements to the crossover point. As there are two pairs of elevations (ascending track ele-

2.5 Elevation change

vation at t1 (h_{At1}) and descending track elevation at t2 (h_{Dt2}) as well as ascending track elevation at t2 (h_{At2}) and descending track elevation at t1 (h_{Dt1}) at one crossover, elevation difference at each point is defined as a mean of these two:

$$Dh(x, t_1, t_2) = \frac{(h_{At1} - h_{Dt2}) - (h_{At2} - h_{Dt1})}{2} \qquad \textit{[Eq. 10]}$$

To generate timeseries of elevation differences we designate one cycle as a reference cycle at time t_{ref} where t refers to the time at the middle of repeat cycle and cross that cycle with each other cycle, so that the elevation difference timeseries can be given by:

$$Dh(x, t, t_{ref}) = \left[\frac{(h_{At} - h_{Dtref}) - (h_{Atref} - h_{Dt})}{2} \right]_{t=t1, t2, t3 \ldots tN} \qquad \textit{[Eq. 11]}$$

In order to reduce errors, elevation differences are binned into 10 km^2 cells and then averaged (Fig. A10b in the Appendix). The number of crossovers per cell is a strong function of latitude being as low as one or zero at latitudes near 65° N and increasing with latitude.

Binned elevation differences for Arctic areas provided by UCL are read into the Matlab software package. Only points inside given glacier outlines provided as a shapefile by GLIMS or WP1 are cropped for trend analysis. For this purpose, elevation differences $dH(x, t, t_{ref})$ using different reference orbits are combined into one set of points $dH(x, t)$ by removing mean elevation difference at each point x for every reference track t_{ref} used. The dH values which deviate more than three times the standard deviation of dH over time in one 10 km^2 cell are discarded as it is suggested by UCL. After the 3-sigma clipping a first degree polynomial is fitted to the time series of elevations, with its slope representing the elevation trend dz/dt.

There are many error sources contributing to the radar altimeter measurement, including radar speckle, topographic noise introduced by sub-footprint changes in elevation and penetration of signal into snow. As all of the error sources are functions of time and place and in general poorly known, overall contribution of these errors to the uncertainty in elevation trend is unknown. Thus, it is more useful to derive an estimate of error from variation of dH measurements over time instead of using formal error estimates of single measurements. The error estimate for the elevation trend in x over the observation period is defined as:

$$e_{(dz/dt)} = \frac{\underset{i=1,2,3\ldots}{std}\ (dH(x, t_i))}{max(t) - min(t)} \qquad \textit{[Eq. 12]}$$

The last step of the processing chain is to write the output variables including elevation difference, time, geographical coordinates of the centre of the averaging cell, elevation trend and the error estimate of the elevation trend into a product shapefile. Data fields of WP4 RA2 elevation change product are presented in Table 6. If the projection of WP1 glacier outline product used is not in geographic coordinates, the ogr software suite will be used to reproject the elevation change product to comply with the WP1 product and the agreed projection system.

Symbol	Explanation	Data type
t	Time (years)	N element vector
dH	Mean measured elevation difference [m] inside averaging cell at time t.	N element vector
dz/dt	Elevation trend [m/y]	Number
e_dz/dt	Estimated error in elevation trend [m/y]	Number
r	Averaging radius used [m]	Number
Lat	Latitude of centre of averaging cell [degrees]	Number
Lon	Longitude of centre of averaging cell [degrees]	Number

Table 6: Data fields of the Envisat RA2 elevation product.

2.6 Velocity

Velocity fields for glaciers will be obtained either from feature tracking of repeat optical imagery (Kääb and Vollmer, 2000) or from microwave sensors using differential SAR interferometry or offset-tracking (Strozzi et al., 2002 and 2007). This section describes workflows of data processing, which can be divided in several logical steps. For simplicity we generally distinguish between three phases of processing, as detailed in Fig. 16. For each step standard algorithms and methods are employed and engineering tests are defined for quality control.

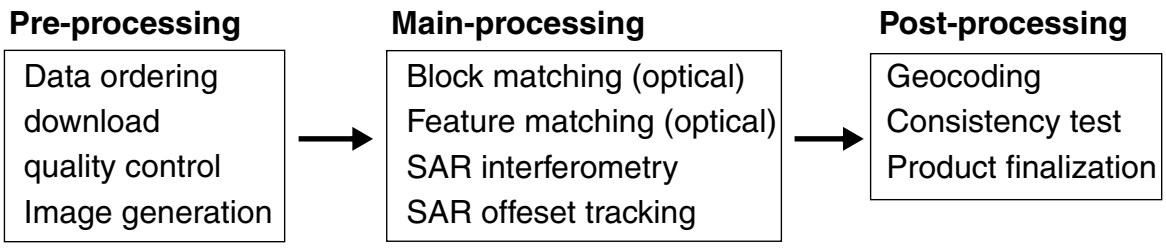

Fig. 16: Schematic overview of the data processing steps for the glacier velocity products.

2.6.1 Optical sensors

The principal for ice velocity measurements based on repeat optical image data is cross-correlation between image blocks from the repeat images (block matching). In Fig. 17 a schematic overview of the processing workflow is given.

2.6 Velocity

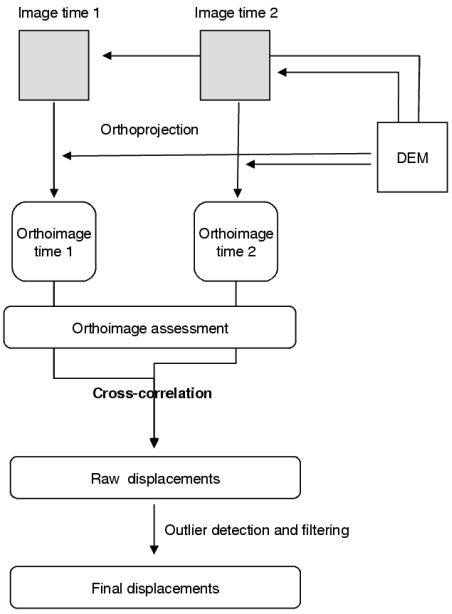

Fig 17: Schematic workflow for generating velocity fields from optical imagery.

Phase 1: Preprocessing

Data selection, ordering and download

The major data sources for correlation between repeat optical images within GlobGlacier will be ASTER, Landsat ETM+ and SPOT. In selected cases ALOS PRISM and AVNIR data will be used. The available scenes are searched and ordered in the USGS glovis (glovis.usgs.gov) and EOLI-SA. In order to be suitable for displacement matching on glaciers, satellite scenes have to fulfil the following requirements (Kääb et al., 2005b, 2006):

- The total displacement in the time interval between the two images used should significantly exceed the spatial resolution of the images
- The glacier or glacier group investigated has to show pronounced features of optical contrast such as crevasses, debris features etc. This implies that image matching does usually not work over snow-covered or firn-covered accumulation areas.
- During the time interval between the two image acquisitions the surface changes have to be small enough to allow identification of corresponding contrast features over the interval.

In addition, the seasonal resolution of the ice velocity measurements has to be observed. According to the above requirements, it may be possible within GlobGlacier to measure summer/winter velocities, annual velocities and/or pluri-annual velocities. Often, the measurement of all three types is not possible due to above requirements and availability of sufficient images.

2.6 Velocity

Raw data quality control
The suitability of repeat image data for matching can usually be fully assessed only based on the full-resolution data. The degree of optical contrast and availability of corresponding features between the repeat data is visually assessed using image viewer zoom functions. If suitable, the scenes are further processed.

Orthoprojection
Orthoprojection of the repeat image data to be correlated ensures that the displacements matched stem from actual ice displacement, rather than, for example, differential topographic distortions between the images.

Orthoimage control
Horizontal distortions in orthoimages directly cause errors in displacements matched from them. The quality controls of the orthoimages include (see also 2.4):

- Create DEM contours, overlay them on the orthoimages and visually check for errors and artifacts. Indications for orthoimage errors are sections where the topographic features have a horizontal offset between the image and the DEM.
- Drape the orthoimage over the DEM and check through 3D visualisation or fly-throughs for areas where image and DEM do not correspond.
- Compare the orthoimages of the ASTER nadir channel 3N and the backward channel 3B. For an DEM free of vertical and horizontal errors, the 3N and 3B orthoimages should perfectly overlap. On the other hand, horizontal shifts between the two orthoimages are a clear indication of DEM errors in the respective terrain sections. The underlaying DEM error can be estimated from the horizontal shifts at distinct places by dividing the shift through the stereo ration of the sensor, in case of ASTER about 0.6 (Kääb, 2002 and 2005a). Similar DEM tests can be performed using ALOS PRISM stereo pairs or triplet image sets.
- Overlay the two orthoimages produced for later matching and analyze distortions over stable terrain or apparently unrealistic distortions over glaciers with respect to distortion/displacement direction and magnitude.

Depending on the outcome of the above quality assessment, the orthoimages are accepted, reprocessed using improved input parameters, masked in order to exclude erroneous sections, or fully declined.

Phase 2: main processing (image correlation)
For image correlation the software CIAS is used (Kääb and Vollmer, 2000). A processing polygon or a list of manually selected individual points are generated where correlations between the two repeat images are to be computed. In the first case, a regular grid width is chosen where the cross-correlation will be computed. In the second case, cross-correlations will be computed for a irregular network of locations. Usually, a regular grid is the approach of choice for glaciers or glacier sections that show a large number of features with optical contrast, such as heavily crevassed glaciers or glaciers with (partial) debris cover. For glaciers or glacier sections with only few contrast features, manual selection and subsequent automatic cross-correlation for these points is more efficient because the effort for post-processing and error detection becomes otherwise too large.

2.6 Velocity

For each location measuring an individual horizontal displacement vector basically follows two steps: (1) In the orthophoto of time 1 an image section (so-called 'reference-block') is chosen by manual selection or as grid point. The ground co-ordinates of its central pixel are known from the orthophoto geo-reference. (2) The corresponding image section (so-called 'test-block') is searched for in a sub-area (so-called 'test-area') of the orthophoto of time 2. If successfully found, the differences in central pixel co-ordinates directly give the horizontal displacement between time 1 and 2.

For identifying corresponding image blocks in both images a double cross-correlation function based on gray values of the images is used:

$$\Phi(i,k) = \frac{\sum_j \sum_l \mathrm{s}\left((i+j,k+l) - \left(\frac{\mathrm{T}_{\mathrm{test}}}{\mathrm{N}_{\mathrm{test}}}\right)\right) \cdot \mathrm{m}\left((j,l) - \left(\frac{\mathrm{T}_{\mathrm{ref}}}{\mathrm{N}_{\mathrm{ref}}}\right)\right)}{\sqrt{\sum_j \sum_l \mathrm{s}^2\left((i+j,k+l) - \left(\frac{\mathrm{T}_{\mathrm{test}}}{\mathrm{N}_{\mathrm{test}}}\right)\right) \cdot \sum_j \sum_l \mathrm{m}^2\left((j,l) - \left(\frac{\mathrm{T}_{\mathrm{ref}}}{\mathrm{N}_{\mathrm{ref}}}\right)\right)}} \qquad \textit{[Eq. 13]}$$

where Φ is the double cross-correlation function, (i, k) and (j, l) are the co-ordinates inside the test- and reference-block, s is the spatial grey-value function of the test-block, $s(i, k)$ is the corresponding grey value at location (i, k), m is the spatial gray-value function of the reference-block, $m(j, l)$ is the corresponding grey value at location (j, l), T is the sum of grey values of the test- or reference-block, and N is the number of pixels of the test- or reference-block (N_{ref}=N_{test}). The global maximum of Φ is supposed to indicate the displaced terrain block of time 1. The T-over-N terms in the equation normalize the gray values of test- and reference-blocks and ensure that differences in overall gray value do not affect the correlation result.

The size of the test-area has to be chosen according to the expected maximum displacement, so that the test-block which corresponds with the reference-block can, in fact, be found in the test-area. The size of the reference- and test-block has to be chosen according to the textural characteristics of the ground surface. If the block sizes are too small, Φ has no clear maximum; if the block sizes are too large, computing time soars drastically. Typical image-block sizes range from 7 x 7 pixels to 31 x 31 pixels.

The result of the matching process is a point list containing point co-ordinates at time 1, the co-ordinates of the corresponding ground points at time 2, x- and y-coordinate differences, displacement magnitude and direction, and the correlation coefficient for each measurement.

Phase 3: post-processing

Outlier detection and filtering

Depending on the image quality and suitability of the surface features for cross-correlation the raw measurements contain a number of mismatches. Within GlobGlacier the following filters will be applied to identify and eliminate such errors:

- Adaptive selection of a threshold correlation coefficient for the displacement measurements to be accepted. Its value differs from case to case and is chosen interactively by visual inspection.
- Filtering using thresholds for (minimum and) maximum displacement magnitude.
- Filtering using a threshold sector for the displacement direction; such a sector can be defined section-wise if needed.
- If necessary neighbourhood analysis will be applied through a median filter or comparison of measured values to interpolated ones.
- Finally, a few remaining obvious measurement outliers will be removed manually in an GIS environment.

All the above steps are performed using basic ArcGIS editing capabilities and ArcGIS Spatial Analyst.

Product finalizing
In this step the final data products are formatted, documented and delivered. Compliance of the product with the specifications of the offered service is checked.

2.6.2 Microwave sensors

Pre-processing

Data selection, ordering and download
The major data sources for the glacier velocity products are ERS-1/2 SAR, ENVISAT ASAR and ALOS PALSAR data obtained from ESA through an IPY AO (principal investigator: T. Strozzi). The available scenes are searched with EOLI-SA with respect to acquisition data, acquisition time interval and baseline. Orders are placed directly in EOLI-SA and data download is performed via FTP. SAR raw data to be processed with the Gamma software are typically considered. Basic steps of the processing are illustrated in Fig. A11 in the Appendix.

Data quality control
The raw data quality control is done using the Gamma MSP software. This step includes the check of SAR raw data for missing lines, and, if available, the addition of precision orbit state vectors. If multiple frames of the same orbit are ordered, SAR raw data are concatenated.

SAR processing
The SAR processing is done using the Gamma MSP software (see Fig. 10). The SAR processing step includes Doppler centroid estimation and optimization, autofocus, and radiometric calibration. The Doppler centroid estimation is checked by the first two components of the Doppler polynomial with the first component expected in the range of [-2000 ... 2000 Hz]. The autofocus step is assured by the SNR and the Doppler ambiguity error estimate. The SNR must be larger than 4, and the absolute value of the ambiguities smaller than 0.1. The radiometric calibration is checked by the average backscattering coefficient. For multiple scenes the values are expected to be within 1 dB. Higher differences may occur in the case of wind roughed water surfaces, changing snow signatures and freezing/thawing.

Main processing (SAR interferometry)

Co-registration of SAR images

In preparation of the interferogram generation the SLC images need to be registered to a common geometry at sub-pixel accuracy. The quality of the co-registration is determined during the derivation of the range and azimuth offset polynomials. As quality measures the standard deviation of the individual offset estimates from the polynomial fits for the range and azimuth offsets are used. These standard deviations must be in the sub-pixel domain (e.g. < 0.5 pixel), otherwise the registration step must be redone.

Interferometric processing

The interferometric processing is done using the Gamma ISP software (Fig. 18). It includes the baseline estimation and the interferogram flattening (the removal of the orbital phase trend). The quality of the interferogram is visually checked by the operator.

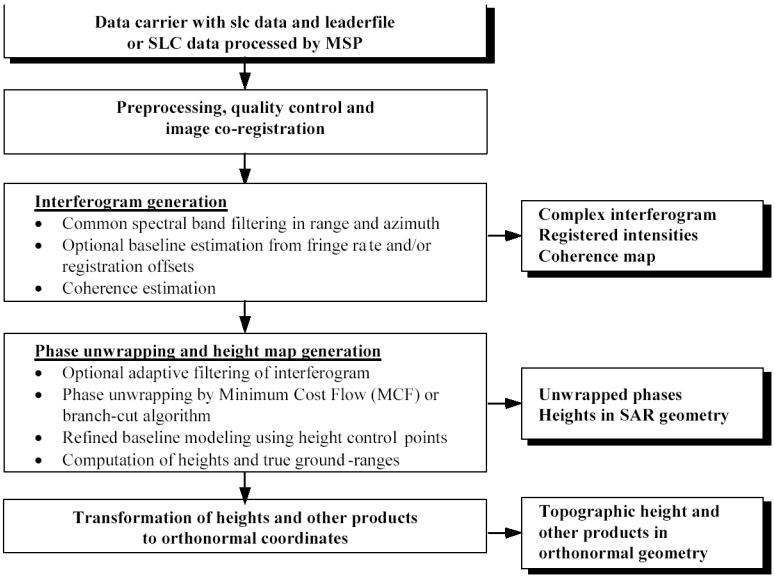

Fig. 18: Flowchart of the ISP software.

Preparation and subtraction of topographic phase component

The topographic phase component is either derived based on a DEM in the so-called 2-pass approach (Fig. 19), or based on two independent interferometric pairs in the multi-pass approach (Fig. 20). In the first case terrain corrected geocoding is required (with the standard deviation values in the fine registration step as an important characteristic of successful processing). The unwrapped interferometric phase is then derived from the terrain height values and the interferometric baseline.

2.6 Velocity

In the second case an independent interferometric pair needs to be processed and the combined interferogram unwrapped. The unwrapped interferometric phase needs to be scaled to represent the topographic phase for the baseline configuration of one of the interferograms. Apart from the individual checks described in this step an integrated quality control is conducted in the visual check of the differential interferogram. The "flatness" achieved for stable areas is a good characteristic of the baseline estimation accuracy.

Phase unwrapping
Phase unwrapping could be difficult and is not always straightforward. For this reason the testing of the quality of the unwrapping is very important. The operator selects between different filtering and unwrapping approaches. Once unwrapping was successful the result is critically investigated for phase unwrapping errors. Based on this the operator can decide to accept the result, to mask out areas of unreliable information and then to accept the result or to redo the phase unwrapping with a modified approach tuned to avoid the problems which occurred.

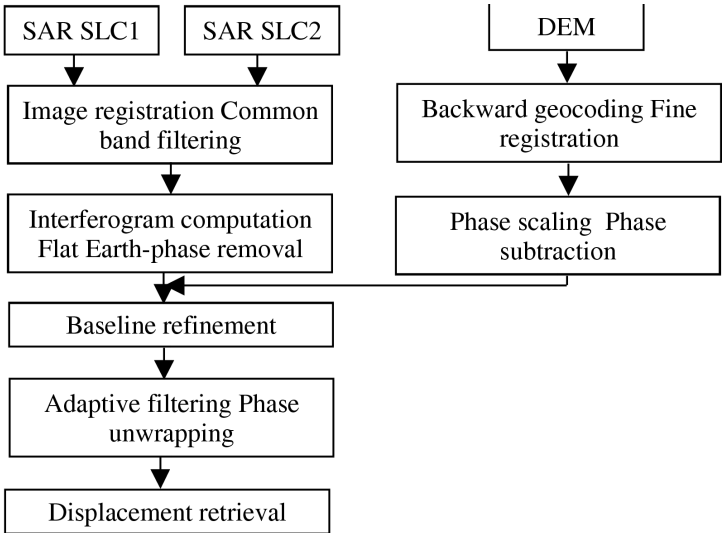

Fig. 19: Flow chart for 2-pass differential SAR interferometry.

Displacement retrieval
Once an unwrapped differential interferogram is available, the surface displacement map can be generated. The differential interferometric phase corresponds to the displacement along the SAR look vector. As a consequence the 3-dimensional (3D) displacement of a surface element cannot be completely described. Under the assumption of an indicated direction field (e.g. along the height gradient) the 3D displacement field can be computed from one InSAR-based line-of-sight displacement component. Two InSAR-based line-of-sight displacement components from ascending and descending orbits can be used to calculate the 3D displacement field based on the surface parallel assumption. In both cases the output displacement field is expressed through the norm, the elevation angle (theta) and the orientation angle (phi).

2.6 Velocity

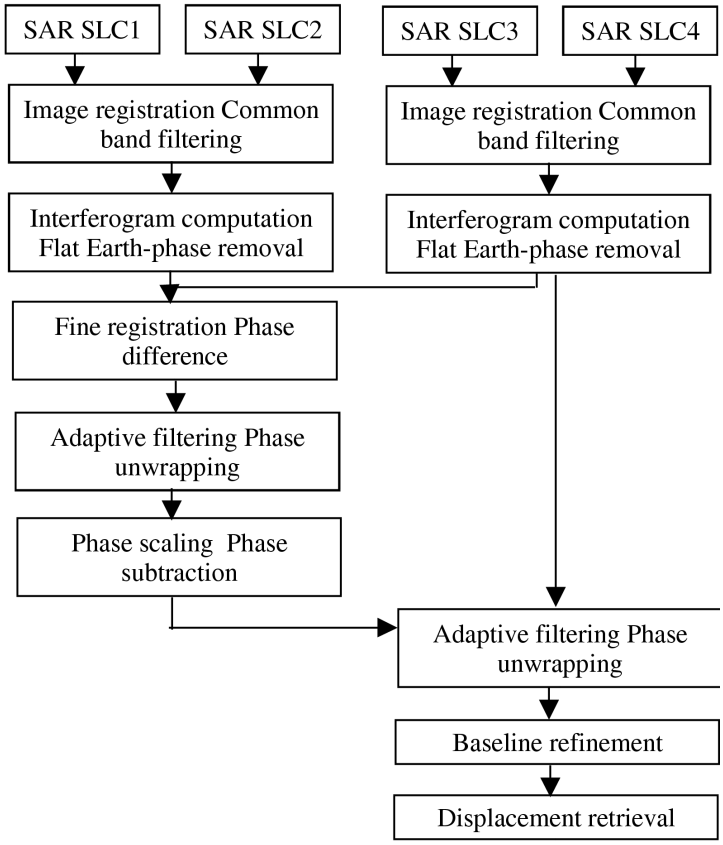

Fig. 20: Flow chart for 4-pass differential SAR interferometry.

SAR offset-tracking

Co-registration of SAR images

In preparation of offset-tracking the two SLC images need to be registered to a common geometry at sub-pixel accuracy (Fig. 21). The quality of the co-registration is determined during the derivation of the range and azimuth offset polynomials. As quality measures the standard deviation of the individual offset estimates from the polynomial fits for the range and azimuth offsets are used. These standard deviations must be in the sub-pixel domain (e.g. < 0.5 pixel), otherwise the registration step must be redone.

Precise estimation of offsets

Once the bilinear polynomial function is known, many offsets are estimated in the area of interest based on the image intensity cross-correlation using the Gamma ISP software. The bilinear polynomial function obtained at the previous stage serves as indication for the position where to estimate the precise offsets. The field of registration offsets here obtained correspond to the offsets in range and azimuth. Quality measures are also computed. The selection of a search window size, an oversampling factor, and of the SNR level depends on the size of the area of interest, on the number of estimates, and on the expected accuracy.

Displacement retrieval
The pixel offsets estimated in range and azimuth direction are transformed to displacements. The bilinear polynomial function determined all over the image is used for the separation of the orbital offsets from those of the area concerned with displacement. Points can be rejected based on a SNR thresholding. Further refinement is possible with filtering of noise and azimuth streaks. The displacement components from range and azimuth direction can be used to calculate the 3D displacement field based on the surface parallel assumption. In both cases the output displacement field is expressed through the norm, the elevation angle (theta) and the orientation angle (phi).

Post processing
Geocoding
SAR terrain corrected (or ellipsoid corrected if no DEM is available) geocoding is the geometric transformation from slant range into the product geometry. This step is done using the Gamma DIFF&GEO software (Fig. 21). Standard deviations in the fine registration step and visual inspection are used as engineering tests. A mosaic of different frames covering the same area can be accomplished after geocoding.

Consistency testing
By visual inspection the operator conducts consistency tests to evaluate the credibility of the result(s) (sign, level, location, geometry of deformation). Multiple independent results and independent measurements are very useful in this step, if available.

Product finalizing
In this step the final data products are formatted, documented and delivered. Compliance of the product with the specifications of the offered service is checked.

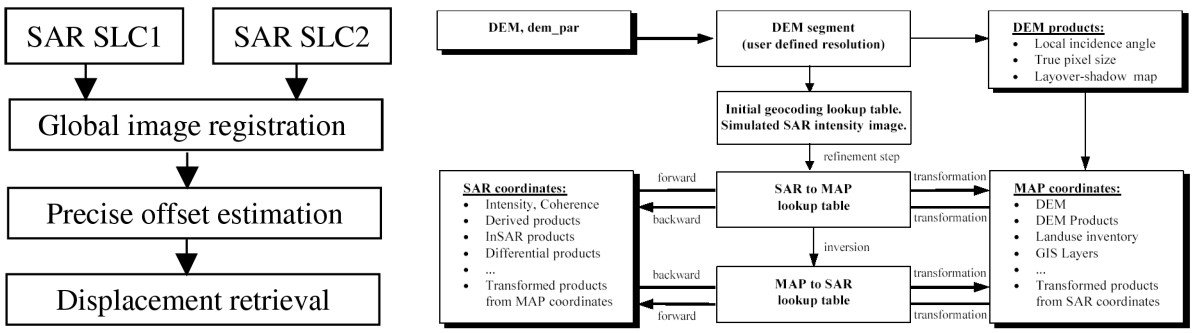

Fig. 21: Flow chart for SAR offset-tracking (left) and flow chart of the SAR geocoding with the DIFF&GEO software (right).

3. Integrated information products

3.1 Data exchange and formats in the consortium

In order to generate integrated information products, data exchange have to be organized within the consortium. As details of this exchange are described in the minutes of the second progress meeting in Innsbruck, we here only repeat the most important points. In order to facilitate data exchange among the consortium, a shared hard disk and a user account has been established for the computer infrastructure at GIUZ. Data formats includes three topics: file format, file contents and file names. For the file formats the following rules are used

- The shape file format will be used for vector data, (polygon and point) with the data stored in the attribute table.
- The GeoTif format will be used for raster data as it can store projection information.
- For each region, the projection of the respective orthorectified Landsat scenes is used (UTM with zone and WGS84 datum). Some overlap could result for mosaiced DEM tiles.
- Metadata and other related information will be exchanged in ASCII format (.met, .txt, .dat).
- Raw data like Landsat scenes or SRTM tiles will not be exchanged on the disk

File naming conventions will follow established rules. Some meta-information (sensor, location, date, product) will be a part of the file name. The principle structure of the file name is: product_region_date_sensor. Suggested abbreviations for sensor and product names are listed in Table 7. The format of the date is YYMMDD, the region is abbreviated with the identifier from the respective sensor. In the case of optical satellite data it will refer to a path and row numbering scheme, for the other sensors it will refer to an analogue identifier. For example, a glacier outline derived from a Landsat 5 TM scene will have the name: gl013011_010804tm with the suffixes .shp, .shx and .dbf (and .prj where available).

Sensor	Abbrev.
Landsat MSS	mss
Landsat TM	tm
Landsat ETM+	etm
ASTER	ast
SPOT	sp
IRS	irs
Quickbird	qb
Ikonos	iko
Corona	cor

Sensor	Abbrev
ERS1/2	esar
ASAR	asar
Palsar	psar
ICESat	ice
RA2	ra2

Product	Abbrev.
Outline	gl
Terminus	tp
Snowline	snl
Topography	dtm
Elev. change	elc
Velocity	vel

Table 7: Suggested abbreviations (Abbrev.) for sensor and product names.

The contents and format of each file will vary with the product (see Table 8). The **glacier outline** product will consist of a set of polygons with a unique identifier. For the internal data exchange, this product will not include all specifications of the GLIMS database. This format will be created after all other product details are integrated (see 3.2). The **terminus position** will consist of a shape file with the glacier id, coordinates (x, y) and, where available, elevation (z). The file name will link the dataset to a specific satellite scene / time stamp. The **snow line** will be provided in two formats, a black/white raster image (GeoTiff) showing the classification results and a vector line representing the snow line. **Topography** as derived from any sensor will be an image in GeoTif format. **Elevation changes** will also use two formats: a point shape file will consist of spot elevation changes (incl. glacier IDs and time stamps) and GeoTiffs will be used for raster data as derived from DEM subtraction. The velocity product will be provided in a (maybe regularly spaced) point shape file that includes the glacier ID, displacement values in x, y, and z and time stamps.

Product	Outline	Terminus	Snow line	Topography	Elev. change	Velocity
Format	shp vec	shp pt	shp v ec + GeoT	GeoT (ASCII)	shp pt, GeoT	shp pt
Contents	polygon, ID, attributes	glacier ID, x,y,z coord.	polygon + binary image	image	ID, value (m), time stamps	ID, displacement in x/y,/z time stamps

Table 8: File formats and contents. Shp: shape, vec: vector, pt: point, GeoT: GeoTiff.

3.2 Integrated data products for the user group

The data submitted to the GLIMS and WGMS databases will have different formats. The exact specifications are described in the Appendix of the RB. One main difference is that all results have to be converted to geographic coordinates (WGS84 datum) and that rock outcrops within a glacier must have the id of the glacier while rock outcrops which are shared by two or more glaciers have a zero entry.

Additionally, the raw product data as generated and exchanged by the GlobGlacier consortium will also be down-sampled for the database submission. This means that raster data (GeoTiffs) will not be included directly but derived products are provided in the attribute table of the respective glacier. For example, only scalar numbers will be given for each glacier from the DEM (e.g. min/max/mean elevation, 100 m hypsography) and elevation changes will be given as a mean over discrete elevation bands (along with the hypsography) or for the entire glacier. This will also allow to be compliant with copyright restrictions for national DEMs.

The exact format of the L0 outlines have to be specified in the future. At the moment the GLIMS database requires to have a unique code for each glacier entity, which is only applicable for the L1 and L2 outline product. The L0 product might have an independent coding format or a simple yes/no (binary) coding scheme for all ice masses.

4. Consolidation of the demonstration cases

Due to the changed data policy at USGS, all Landsat data will be available for free in an already orthorectified version from Spring 2009 on, i.e. with the beginning of phase 2. It has also been stated (at the GLIMS workshop in Boulder this year) that the global ASTER DEM will be available for free in Spring 2009. These two datasets together with the DEM from SRTM will form the backbone of the phase two demonstration cases. From this point of view it is most likely that the products quantities envisaged in the proposal could be exceeded for all products.

However, it is also very likely that the GLIMS community will increase its output considerably and overlap of processed scenes will occur in many cases. While this certainly will help to achieve the goal of a global glacier inventory from satellite data, it will cause some trouble in the GLIMS database when identical scenes are processed by different groups. In view of the aims of GlobGlacier this is more a chance than a drawback, as the independent processing of the same scene is still one of the best measures to identify problems, methodological challenges and the accuracy of the data processing. Moreover, glacier outlines will be used within GlobGlacier also internally for several additional products and are processed by a small team according to the same standards. So we assume that they can still serve as a reference.

5. References

Berthier, E., Y. Arnaud, C. Vincent, and F. Rèmy (2006): Biases of SRTM in high-mountain areas: Implications for the monitoring of glacier volume changes. *Geophysical Research Letters*, 33 (8), L08502.

Bishop, M. P., R. Bonk, U. Kamp and J.F. Shroder, Jr. (2001): Terrain analysis and data modeling for alpine glacier mapping. *Polar Geography*, 25(3), 182-201.

Braithwaite, R.J. (1984): Can the mass balance of a glacier be estimated from its equilibrium-line altitude? *Journal of Glaciology*, 30 (106), 364-368.

Chinn, T.J., C Hydenrych and M.J. Salinger (2005): Use of the ELA as practical method of monitoring glacier response to climate in New Zealand's Southern Alps. *Journal of Glaciology*, 51(172), 85-95.

Ekstrand, S. (1996): Landsat TM-Based Forest Damage Assessment: Correction for Topographic Effects. *Photogrammetric Engineering and Remote Sensing*, 62 (2), 151-161.

Gens, R. and J.L. van Genderen (1996): Analysis of the geometric parameters of SAR interferometry for spaceborne systems. *International Archives of Photogrammetry and Remote Sensing* (Vol. XXXI, Part B2). ISPRS, Vienna, pp. 107-110.

Gens, R. (1998). Quality assessment of SAR interferometric data. PhD thesis, University of Hanover, Germany, 141 pp.

Goldstein, R. M., H. Engelhardt, B. Kamb and R. M. Frolich (1993): Interferometry For Monitoring Ice-Sheet Motion - Application To An Antarctic Ice Stream. *Science*, 262(5139), 1525-1530.

Graham, L.C. (1974): Synthetic interferometer radar for topographic mapping. *Proceedings of the IEEE*, 62 (6), 763-768.

Hall, D., K. Bayr, W. Schöner, R. Bindschadler and J. Chien (2003): Consideration of the errors inherent in mapping historical glacier positions in Austria from the ground and space (1893-2001). *Remote Sensing of Environment*, 86(4), 566-577.

Huggel, C., A. Kääb, W. Haeberli, P. Teysseire and F. Paul (2002): Remote sensing based assessment of hazards from glacier lake outbursts: a case study in the Swiss Alps. *Canadian Geotechnical Journal*, 39 (2), 316-330.

Itten, K.I. and P. Meyer (1993): Geometric and radiometric corrections of TM data of mountainous forested areas. *IEEE Transactions on Geosciences and Remote Sensing*, 31(4), 764-770.

Joughin, I.R., D.P. Winebrenner and M.A. Fahnestock (1995): Observations of ice-sheet motion in Greenland using satellite radar interferometry. *Geophysical Research Letters*, 22, 571-574.

Joughin, I., R. Kwok and M. Fahnestock (1996): Estimation of ice-sheet motion using satellite radar interferometry: Method and error analysis with application to Humboldt Glacier, Greenland. *Journal of Glaciology*, 42(142), 564-575.

Joughin, I.R., R. Kwok and M.A. Fahnestock (1998): Interferometric estimation of three-dimensional ice flow using ascending and descending passes. *IEEE Transactions on Geoscience and Remote Sensing*, 36(1), 25-37.

Joughin, I.R., M.A. Fahnestock. and J.L Bamber (2000): Ice flow in the northeast Greenland ice stream. *Annals of Glaciology*, 31, 141-146

Kääb, A. (2002): Monitoring high-mountain terrain deformation from repeated air- and space-borne optical data: examples using digital aerial imagery and ASTER data. *ISPRS Journal of Photogrammetry and Remote Sensing*, 57(1-2), 39-52.

Kääb, A. (2005a): Remote sensing of mountain glaciers and permafrost creep. Schriftenreihe Physische Geographie, Glaziologie und Geomorphodynamik, 48, University of Zurich.

Kääb, A. (2005b): Combination of SRTM3 and repeat ASTER data for deriving alpine glacier flow velocities in the Bhutan Himalaya. *Remote Sensing of Environment*, 94(4), 463-474.

Kääb, A. and M. Vollmer (2000): Surface geometry, thickness changes and flow fields on creeping mountain permafrost: automatic extraction by digital image analysis. *Permafrost and Periglacial Processes*, 11, 315-326.

Kääb, A., F. Paul, M. Maisch, M. Hoelzle and W. Haeberli (2002): The new remote-sensing-derived Swiss glacier inventory: II. First Results. *Annals of Glaciology*, 34, 362-366.

Kääb, A., B. Lefauconnier and K. Melvold (2006): Flow field of Kronebreen, Svalbard, using repeated Landsat 7 and ASTER data. *Annals of Glaciology*, 42, 7-13.

Kääb, A. (2008): Glacier volume changes using ASTER satellite stereo and ICESat GLAS Laser altimetry. A test study on Edgeøya, Eastern Svalbard. *IEEE Transactions on Geoscience and Remote Sensing*, 46 (10), 2823-2830.

Knap, W.H., C.H. Reijmer and J. Oerlemans (1999): Narrowband to broadband conversion of Landsat TM glacier albedos. *International Journal of Remote Sensing*, 20, 2091-2110.

Kwok, R. and M.A. Fahnestock (1996): Ice sheet motion and topography from radar interferometry. *IEEE Transactions on Geoscience and Remote Sensing*, 34(1), 189-200.

Law, K.H. and J. Nichol (2004): Topographic correction for differential illumination effects on Ikonos satellite imagery. *Proceedings of XXth ISPRS Congress*: Geo-imagery bridging continents, Istanbul, Turkey, ISPRS, Vol. 35, Part 3B.

Li, Z., W. Sun and Q. Zeng (1998): Measurements of glacier variation in the Tibetan Plateau using Landsat data. R*emote Sensing of Environment*, 63, 258-264.

Madsen, S. and H.A. Zebker (1998): Imaging radar interferometry. In: F. Henderson and A. J. Lewis (eds.), Principles and Applications of Imaging Radar: Manual of Remote Sensing (3rd edn., Vol. 2, R. A. Ryerson, editor-in-chief). John Wiley & Sons, New York, pp. 359-380.

Massonet, D. and K.L. Feigl (1998): Radar interferometry and its application to changes in the Earth's surface. *Reviews of Geophysics*, 36(4), 441-500.

Mohr, J.J. (1997): Repeat track SAR interferometry; An investigation of its utility for studies of glacier dynamics. PhD thesis, Technical University of Denmark, Copenhagen.

Müller, F., T. Caflisch, and G. Müller (1977): Instructions for the compilation and assemblage of data for a world glacier inventory. IAHS(ICSI)/UNESCO report, Temporal Technical Secretariat for the World Glacier Inventory (TTS/WGI), ETH Zurich, Switzerland.

Nagler, T. (1996): Methods and analysis of synthetic aperture radar data from ers-1 and X-sar for snow and glacier applications. PhD thesis, University of Innsbruck, Austria, 183 pp.

Oerlemans, J. (2001): Glaciers and Climate Change. AA. Balkema Publ., Lisse etc.

Paul (2007): The New Swiss Glacier Inventory 2000 - Application of Remote Sensing and GIS. Schriftenreihe Physische Geographie, Universität Zürich, 52, 210 pp.

Paul, F. (2008): Calculation of glacier elevation changes with SRTM: Is there an elevation dependent bias? *Journal of Glaciology*, 55 (188), 945-946.

Paul, F. and A. Kääb (2005): Perspectives on the production of a glacier inventory from multispectral satellite data in the Canadian Arctic. *Annals of Glaciology*, 42, 59-66.

Paul, F. and W. Haeberli (2008): Spatial variability of glacier elevation changes in the Swiss Alps obtained from two digital elevation models. *Geophysical Research Letters*, 35, L21502 (doi:10.1029/2008GL034718).

Paul, F., A. Kääb, M. Maisch, T.W. Kellenberger and W. Haeberli (2002): The new remote-sensing-derived Swiss glacier inventory: I. Methods. *Annals of Glaciology*, 34, 355-361.

Paul, F., C. Huggel, A. Kääb, and T.W. Kellenberger (2003): Comparison of TM-derived glacier areas with higher resolution data sets. EARSeL Workshop on Remote Sensing of Land Ice and Snow, Bern, 11.-13.3.2002. *EARSeL eProceedings*, 2, 15-21.

Paul, F., C. Huggel and A. Kääb (2004): Combining satellite multispectral image data and a digital elevation model for mapping of debris-covered glaciers. *Remote Sensing of Environment*, 89 (4), 510-518.

Rabus, B., M. Eineder, A. Roth and R. Bamler (2003): The shuttle radar topography mission - a new class of digital elevation models acquired by spaceborne radar. *ISPRS Journal of Photogrammetry and Remote Sensing*, 57(4), 241-262.

Racoviteanu, A.E, Paul, F., Raup, B., Khalsa, S.J.S. and Armstrong, R. (in press): Challenges in glacier mapping from space: recommendations from the Global Land Ice Measurements from Space (GLIMS) initiative. *Annals of Glaciology*, 50 (53).

Raup, B.H. and Khalsa, S.J.S. (2007): GLIMS Analysis tutorial. GLIMS. Online at: http://www.glims.org/MapsAndDocs/assets/GLIMS_Analysis_Tutorial_a4.pdf.

Rott, H. and G. Markl (1989): Improved snow and glacier monitoring by Landsat Thematic Mapper. Proceedings of a Workshop on Earthnet Pilot Project on Landsat Thematic Mapper Applications, ESA SP-1102, 3-12.

Scharroo, R. and P. Visser (1998): Precise orbit determination and gravity field improvement for the ERS satellites. *Journal of Geophysical Research*, 103 (C4), 8119-8127.

Schiefer, E., B. Menounos and R. Wheate (2008): An inventory and morphometric analysis of British Columbia glaciers, Canada. *Journal of Glaciology*, 54 (186), 551-560.

Shuman, C.A., H.J. Zwally, B.E. Schutz, A.C. Brenner, J.P. DiMarzio, V.P. Suchdeo and H.A. Fricker (2006): ICESat Antarctic elevation data: Preliminary precision and accuracy assessment. *Geophysical Research Letters*, 33, L07501, doi:10.1029/2005GL025227.

Strozzi, T., Luckman, A., Murray, T., Wegmüller, U. and Werner, C. (2002): Glacier motion estimation using SAR offset-tracking procedures. *IEEE Transactions on Geoscience and Remote Sensing*, 40 (11), 2384-2391.

Strozzi, T., A. Kouraev, A. Wiesmann, U. Wegmüller, A. Sharov and C. Werner (2008): Estimation of Arctic glacier motion with satellite L-band SAR data. *Remote Sensing of Environment*, 112 (3), 636-645.

Svoboda, F. and Paul, F. (in press): A new glacier inventory on southern Baffin Island, Canada, from ASTER data: I. Applied methods, challenges and solutions. *Annals of Glaciology*, 50 (53).

Törmä, M. and P. Härmä (2003): Topographic correction of Landsat ETM-Images in Finish Lapland. *IEEE International*, 6, 3629 - 3631.

Vermote, E.F., D. Tanré, J.L. Deuzé, M. Herman, and J.J. Morcrette (1997): Second Simulation of the Satellite Signal in the Solar Spectrum, 6S: An Overview. *IEEE Transactions on Geoscience and Remote Sensing*, 35 (3), 675-686.

Wadham, J.L. and A.N. Nuttal (2002): Multiphase formation of superimposed ice during a mass-balance year at a maritime high-Arctic glacier, *Journal of Glaciology*, 48 (163), 545-551.

Werner, C. L., U. Wegmüller and T. Strozzi (2002): Processing strategies for phase unwrapping for InSAR applications. Proceedings of the 4th European Conference on Synthetic Aperture Radar EUSAR 2002, Cologne, Germany, 4-6 June 2002. VDE, Verlag, Frankfurt, Germany, Vol. 1, pp. 353-356.

WGMS (2008): Fluctuations of Glaciers 2000-2005 (Vol. IX). In: Haeberli, W., Zemp, M., Kääb, A., Paul, F. and Hoelzle, M. (eds.), ICSU (FAGS) / IUGG (IACS) / UNEP / UNESCO / WMO, World Glacier Monitoring Service, Zurich, Switzerland: 266 pp.

Zebker, H. A., P.A. Rosen, R.M. Gldstein, A. Gabriel and C.L. Werner (1994): On the derivation of coseismic displacement fields using differential radar interferometry: The Landers Earthquake. *Journal of Geophysical Research*, 99(B10), 19617-19634.

Zwally, H.J., B. Schutz, W. Ablati, J. Abshire, C. Bentley, A. Brenner, J. Bufton, J. Dezio, D. Hancock, D. Harding, T. Herring, B. Mister, K. Quinn, S. Palm, J. Spinhirne and R. Thomas (2002): ICESat's laser measurements of polar ice, atmosphere, ocean and land. *Journal of Geodynamics*, 34, 405-445.

Zwally, H.J., R. Schutz, C. Bentley, J. Bufton, T. Herring, J. Minster, J. Spinhirne and R. Thomas (2003): updated current year. GLAS/ICESat L1B Global Elevation Data V018, 15 October to 18 November 2003. Boulder, CO: National Snow and Ice Data Center. Digital media.

6. Abbreviations

AAR	Accumulation Area Ratio
ALOS	Advanced Land Observing Satellite
ASAR	Advanced SAR
ASTER	Advanced Spaceborne Thermal Emission and reflection Radiometer
CC	Cubic Convolution
DEM	Digital Elevation Model
DJF	Design Justification File
DN	Digital Number
ELA	Equilibrium Line Altitude
ERS	European Remote sensing Satellite
ESA	European Space Agency
ETM+	Enhanced Thematic Mapper plus
GCP	Ground Control Point
GIS	Geographic Information System
GLAS	Geoscience Laser Altimeter System
GLCF	Global Land Cover Facility
GLIMS	Global Land Ice Measurements from Space
GTN-G	Global Terrestrial Network for Glaciers
ICESat	Ice, Cloud and Elevation Satellite
ID	IDentification
InSAR	Interferometric SAR
L0, L1, L2	Level 0, Level 1, Level 2
LIA	Little Ice Age
LOS	Line Of Sight
LSSIA	Late Summer Snow and Ice Area
LSSL	Late Summer Snow Line
MODIS	Moderate resolution Imaging Spectrometer
MSS	MultiSpectral Scanner
NSIDC	National Snow and Ice Data Center
NN	Nearest Neighbour
RA2	Radar Altimeter 2
RB	Requirements Baseline
RGB	Red, Green and Blue
RMS	Root Mean Square
SAR	Synthetic Aperture Radar
SLC	Single Look Complex image
SNR	Signal to Noise Ratio
SoW	Statement of Work
SPOT	System Pour l'Observation de la Terre
SRTM	Shuttle Radar Topography Mission
SWIR	ShortWave InfraRed

TIN	Triangular Irregular Network
TM	Thematic Mapper
TOA	Top Of Atmosphere
USGS	United States Geological Survey
VNIR	Visible and Near InfraRed
WGI	World Glacier Inventory
WGMS	World Glacier Monitoring Service
WP	Work Package

Appendix: Processing examples

The purpose of this section is to illustrate the methods described before with images from the pre-, main- and post-processing. The selected sites have been chosen arbitrarily from the ongoing work and might not be representative for all regions of the world.

A1. Glacier mapping

The examples in Fig. A1 illustrate the spectral properties of the terrain in the three TM bands that will be used for glacier mapping (see section 2.1.1 and 2.1.2). The RGB-composites are shown to illustrate their potential for post-processing, i.e. manual correction of the automatically derived outlines by visual interpretation (see section 2.1.3). While the 321 composite is most useful in identifying ice and snow in shadow, band 432 helps in delineating debris cover and trimlines and bands 543 is used to correct clean glacier ice and identify clouds. In Fig. A2 the thresholding of the ratio image is illustrated using different thresholds and a median filter and Fig. A3 displays some post-processing steps and the resulting level 0 and level 1 outlines.

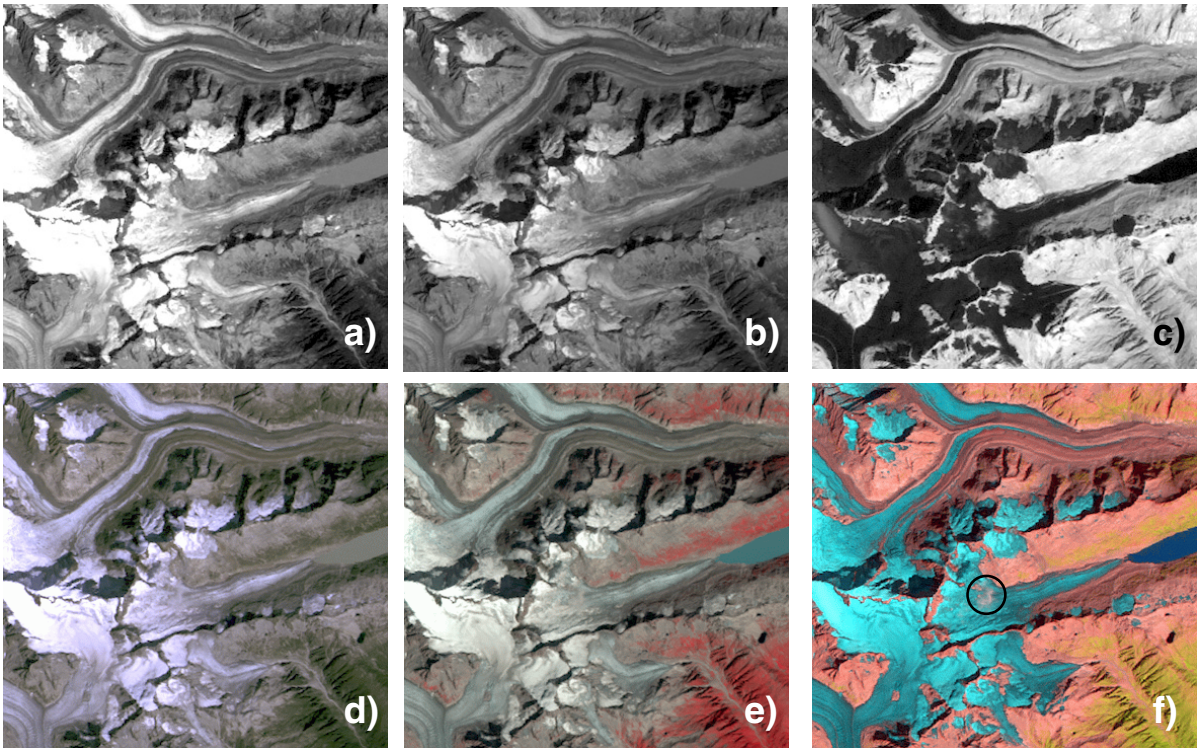

Fig. A1: Subset of a Landsat TM scene around Oberaarglacier in the Swiss Alps (image size is 9.5 km by 9 km, north is at top). a) TM band 1, b) TM band 3, c) TM band 5, d) composite with bands 3, 2 and 1 as RGB, e) bands 4, 3, 2 as RGB and f) bands 5, 4, 3 as RGB. The circle in the latter marks a small cloud.

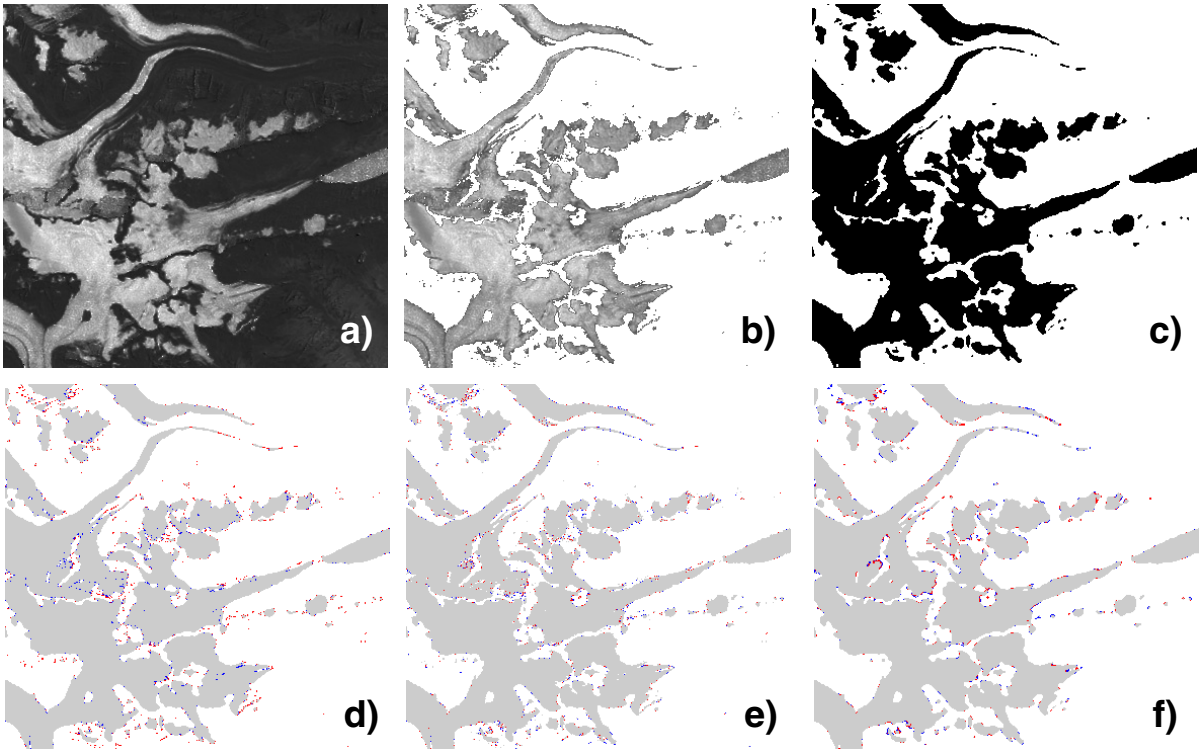

Fig. A2: a) Result of the band ratio, b) after thresholding, c) black and white glacier map, d) effect of a 3 by 3 median filter (removed/added pixels in red/blue), e) three different thresholds (grey: 2.0, grey and red: 1.9, all colours: 2.0), f) as e) but after the median filter has been applied.

Fig. A3: a) Glacier map corrected for debris (light grey) and water bodies represent level 0 outlines, b) glacier basins (bold lines) are used to divide contiguous ice masses, c) individual glacier entities re present level 1 outlines.

A2. Snow mapping

Snow mapping is based on reflectance thresholds which means that the influence of topography on the reflected radiation has to be calculated and removed. Four different methods have been tested for topographic correction (Fig. A4). Results of the classification for the the Jotunheimen region (Norway) and the same test site are depicted in Figs. A5 and A6, respectively.

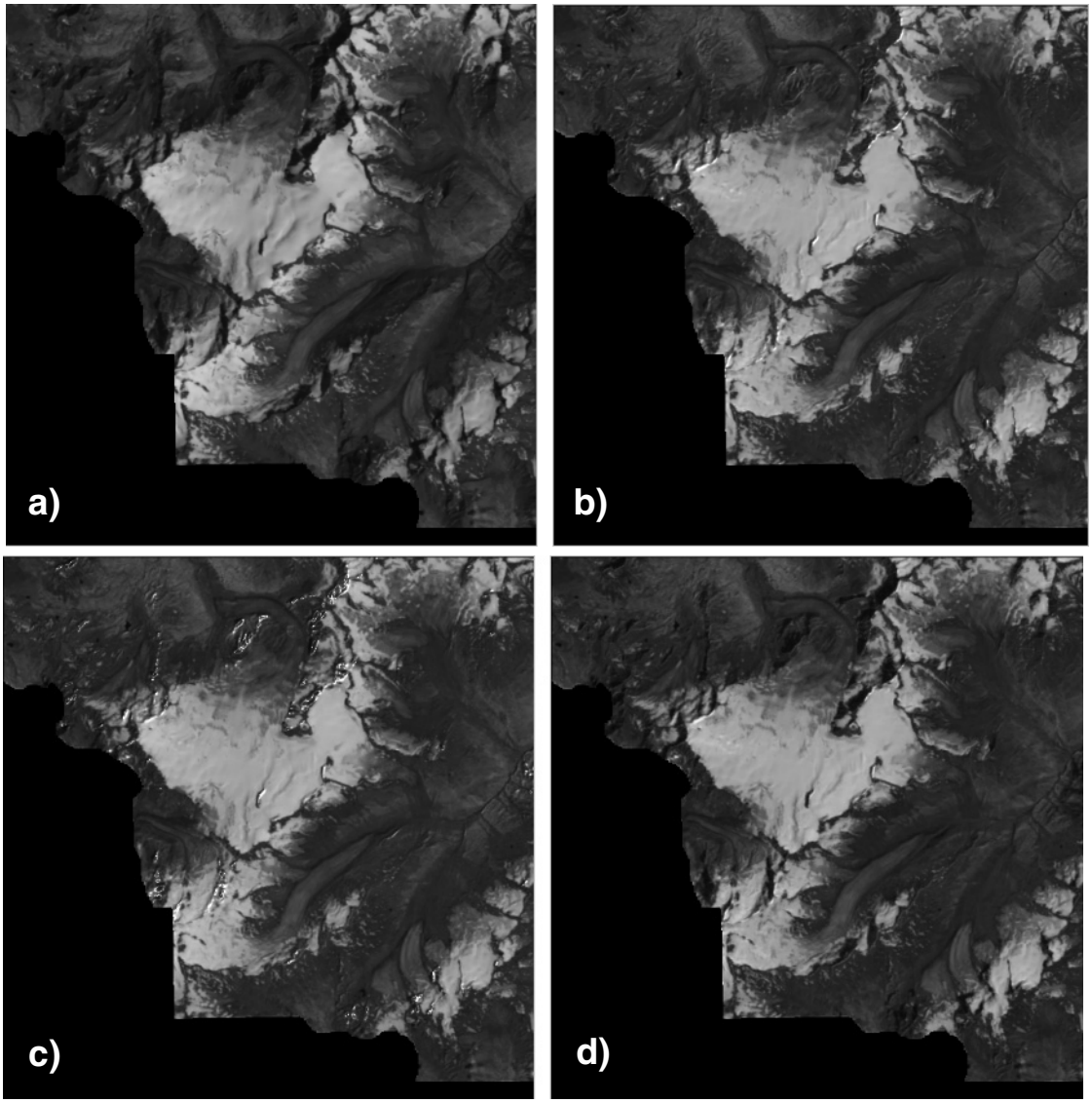

Fig. A4: Landsat 5 TM scene, band 4, of Ötztal Alps, Austria, taken on 16 August 1992, 09:26:42 UTC. a) uncorrected scene, b) C-corrected scene, c) the Minnaert corrected scene and d) the Ekstrand corrected scene. All corrections had been carried out until the constant factor simulated approximately a flat Earth.

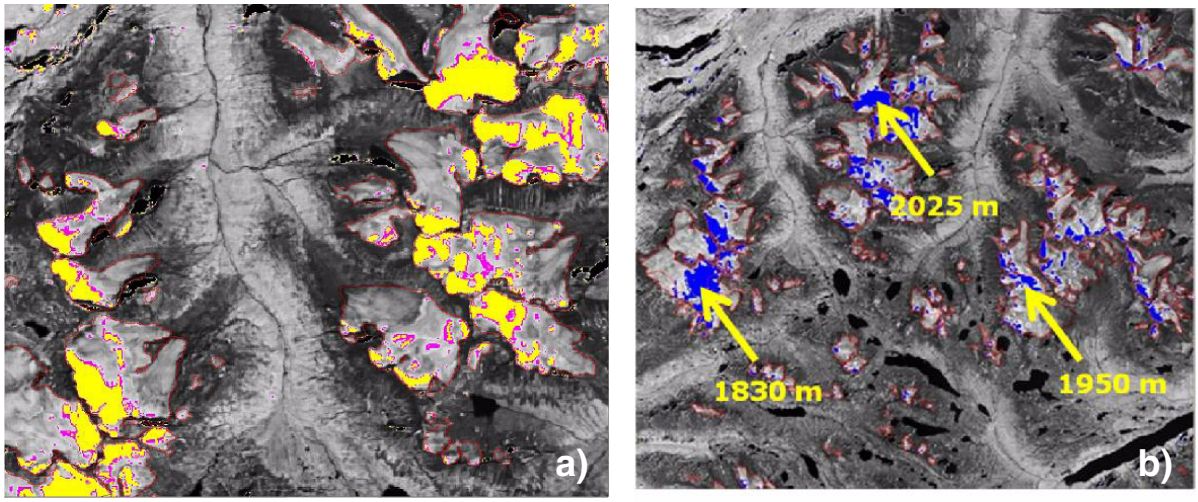

Fig. A5: a) Landsat 5 TM scene, Minnaert corrected (k = 0.453560) band 4 (0.76 - 0.90 m), of test site Jotunheimen / Breheimen, Norway, taken on 09. August 2003. Late summer snow classification using two thresholds of reflectance of snow to consider for superimposed ice: ρ_{snow} *= 0.52 (yellow),* ρ_{supice} *= 0.47 (pink).*

b) *Landsat 5 TM scene, Minnaert corrected (k = 0.45356) band 4 (0.76 - 0.90 m), of test site Jotunheimen / Breheimen, Norway, taken on 09. August 2003. Late summer snow classification using thresholds* ρ_{snow} *= 0.52 and* ρ_{supice} *= 0.47, overlaid with 25 m resolution DEM. Shown examples are mean altitudes of clearly defined LSSL. Values are only valid for a single glacier.*

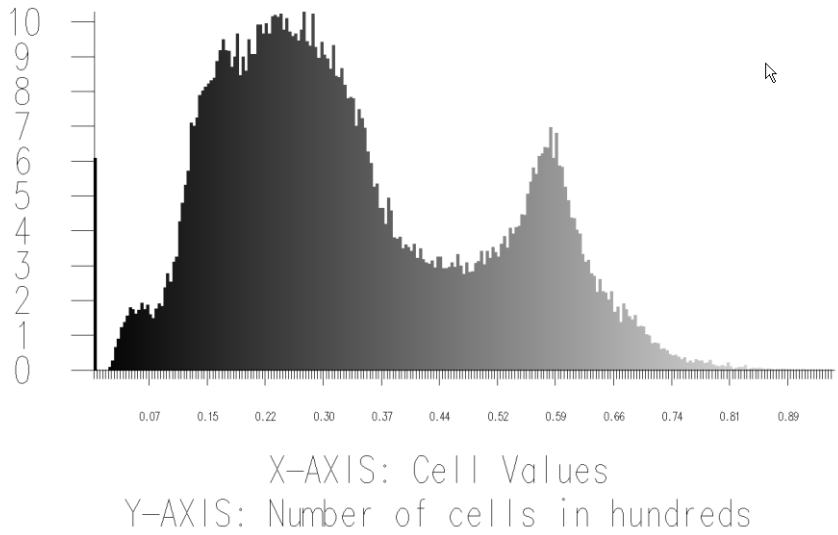

Fig. A6: Histogram of the Ekstrand corrected TOA relectance of band 4 (over glaciers only) for the Landsat ETM+ scene depicted in Fig. A7.

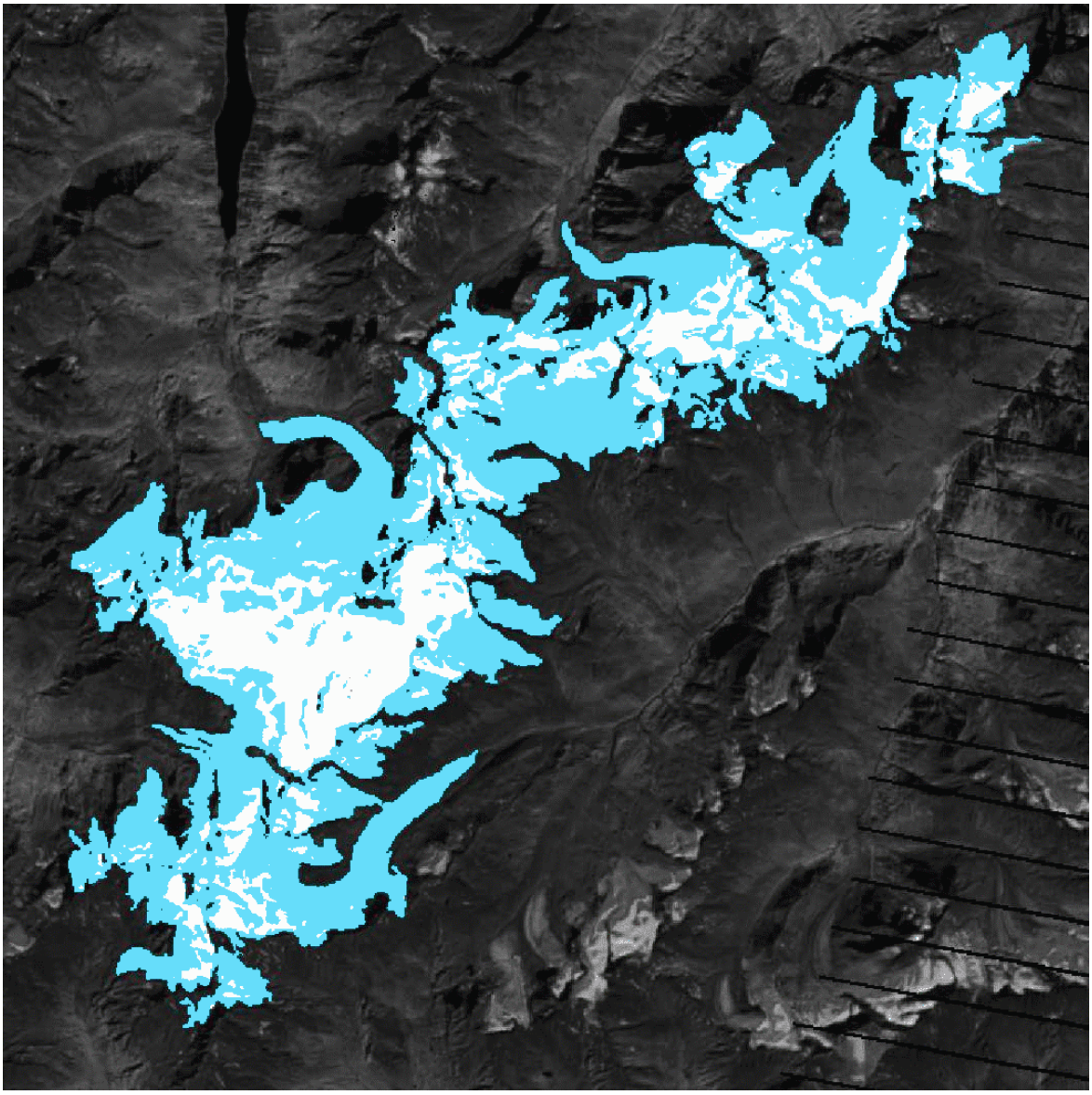

Fig. A7: Classification of bare ice (light blue) and snow (white) for a part of the Ötztal testsite based on Ekstrand corrected ETM+ band 4 TOA reflectance. The threshold value (snow ≥0.44) is based on the histogram depicted in Fig. A6. The black stripes at the right site are due to the malfunction of the scan-line-corrector in ETM+ imagery acquired after June 2003.

A3. Topography

Topographic information is basically derived from the SRTM 3 and the ASTER DEM. For some regions national DEMs are available which are used for quality and change assessment. A direct comparison of the SRTM DEM with an ASTER DEM is depicted in Fig. A8 (highlighting that data voids are at similar locations). Figure A9 illustrates the use of a national DEM (derived from contourlines) for correction of wrongly assigned basin divides from a flowdirection grid.

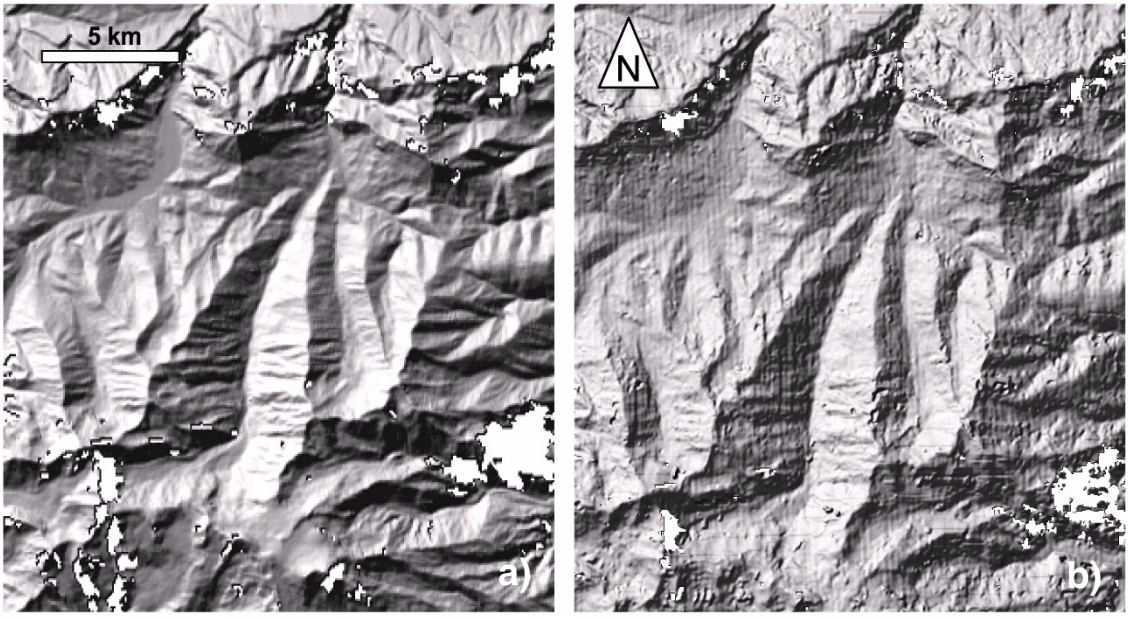

Fig. A8: Comparison of two DEMs (hillshade) in the Caucasus region: a) SRTM3, b) ASTER.

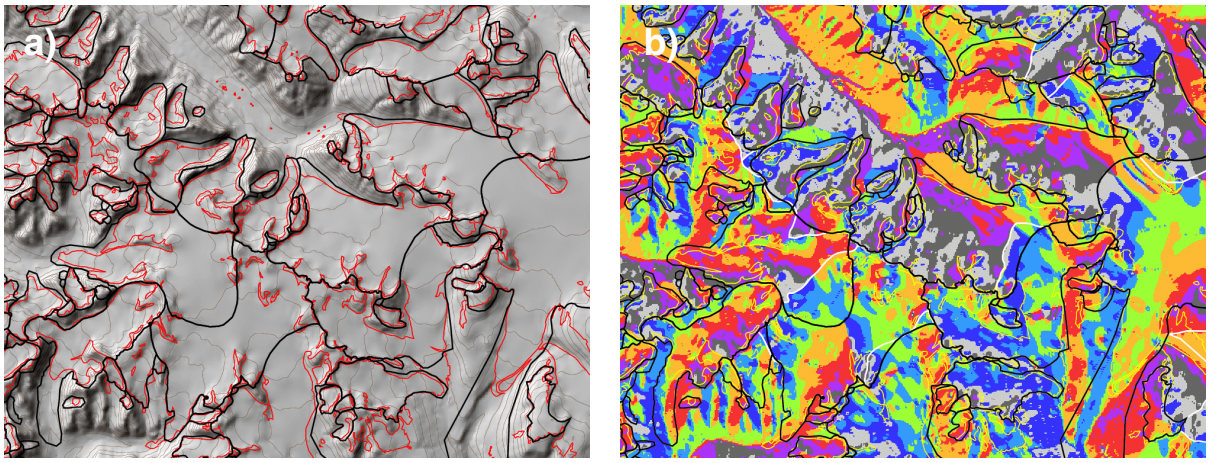

Fig. A9: a) Hillshade of a DEM derived from contourlines for a part of Disko Island (Greenland) with glacier outlines (red) and previously assigned basins (black). b) Colour coded flow-direction grid (8 directions) with manually corrected basin divides (white lines).

A4. Elevation change

Elevation changes will be calculated for point locations (e.g. using ICESat GLAS or EnviSat RA2 data) and entire glaciers (e.g. subtracting two DEMs). A comparison of GLAS elevation points with contourline elevations of a historic topographic map and an ASTER DEM is depicted in Fig. A10. In Fig. A11 elevation changes from DEM subtraction and ICESat GLAS / Envisat RA2 crossover points are illustrated.

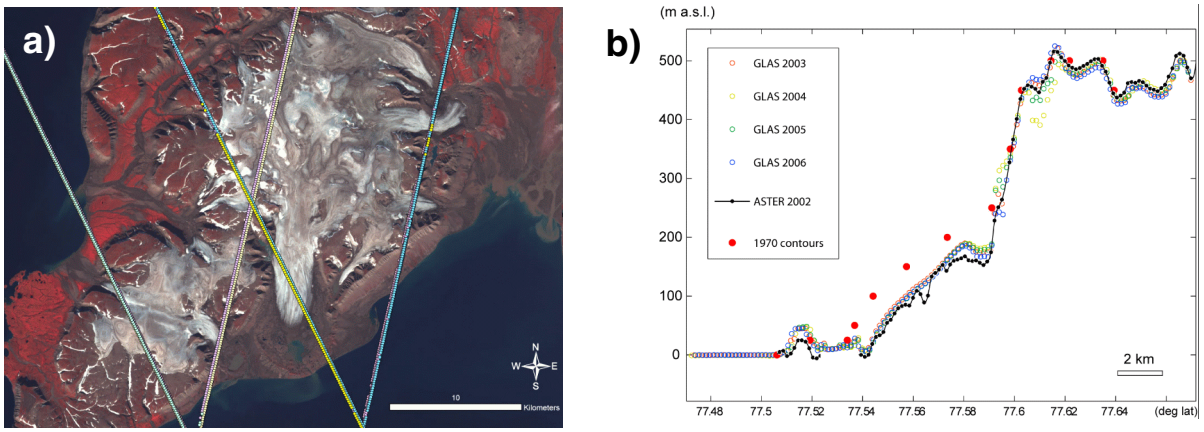

Fig. A10: a) ASTER image with ICESat tracks from the Diggerfonna Icecap on Svalbard. b) Comparison of elevation values along the central profile.

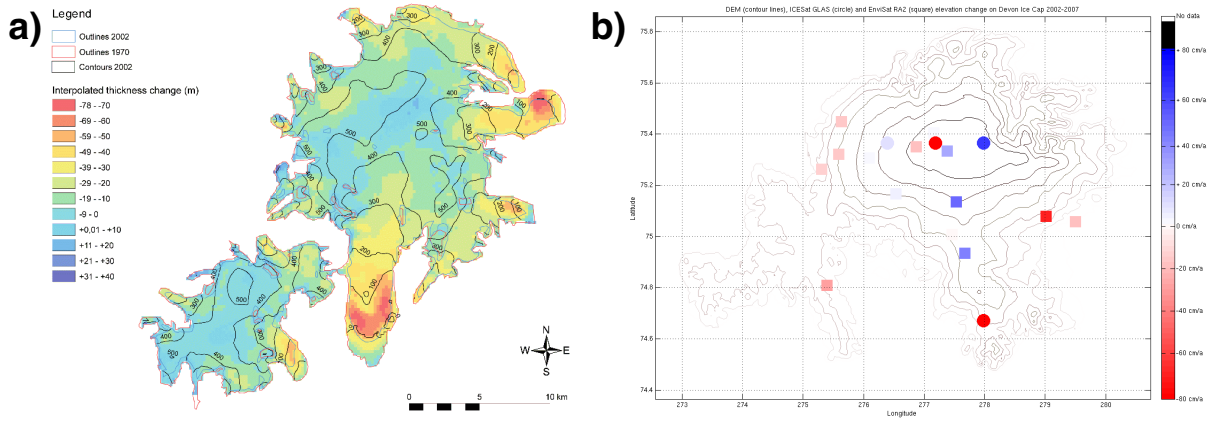

Fig. A11: a) Overall elevation changes for the Diggerfonna Icecap (Svalbard) by interpolating a DEM from the contourlines and subtracting it from the ASTER DEM. b) Averaged point elevation changes from GLAS and RA2 between 2002 and 2007 on Devon Icecap (Canada).

A5. Velocity

The Figures below show image examples for illustration of the processing steps required for deriving velocity fields from microwave data (see Ch. 2.6.2).

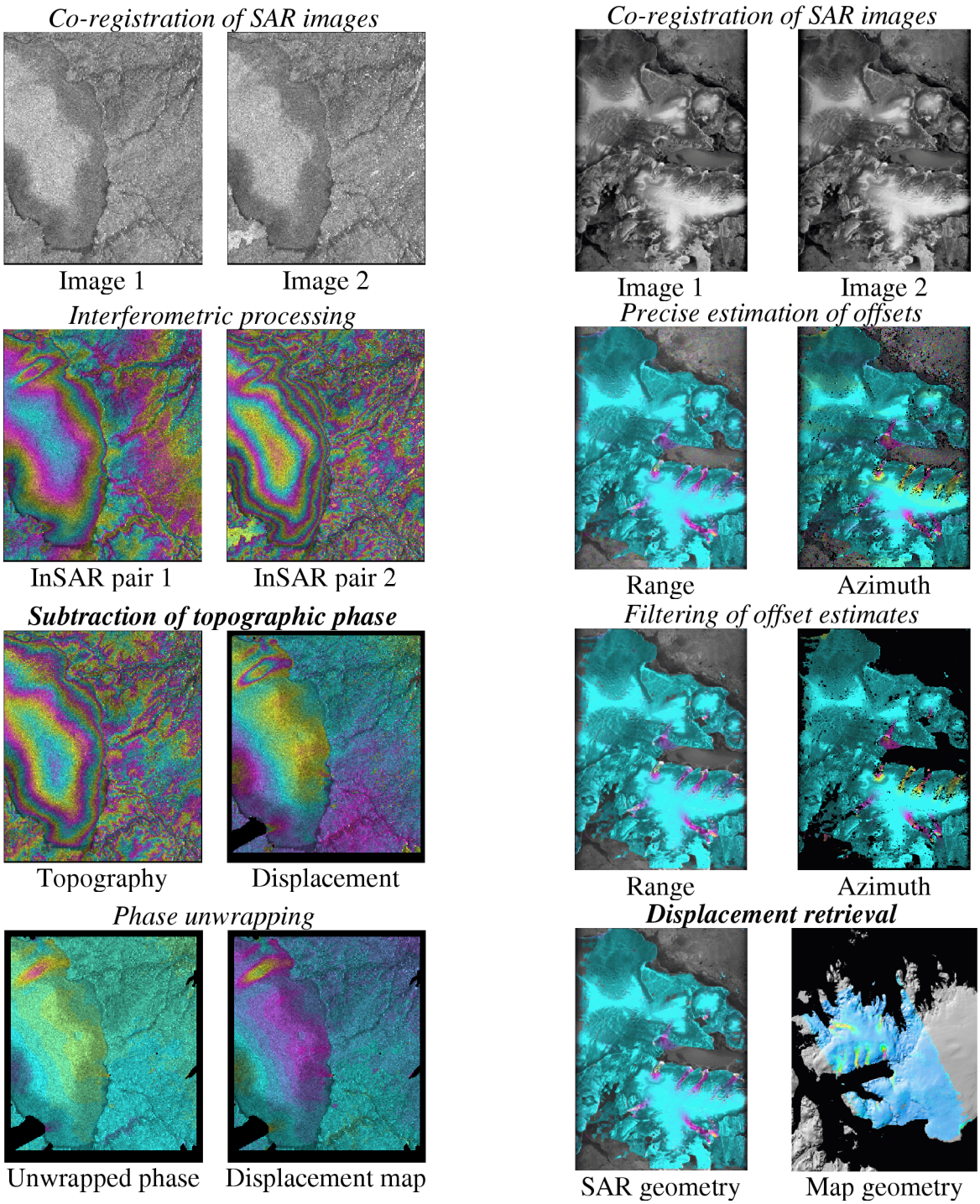

Fig. A12: Illustration of image processing steps for Barnes Icecap (left) and Svalbard (right).